CHAPTER 3

Information Content of Ozone Retrieval Algorithms

Panel Members

C. Rodgers, Chair

P. K. Bhartia
W. P. Chu NDZ10491
R. Curran
J. DeLuisi NJ9209 44
J. Gille NH315709
R. Hudson NC999967
C. Mateer A6530300
D. Rusch
R. J. Thomas
R. Turco
W. Wiscombe

Chapter 3

Information Content of Ozone Retrieval Algorithms

Contents

3.0 INTRODUCTION

All practical methods of measuring atmospheric ozone that are useful for monitoring trends are indirect in some way. The quantity that an instrument measures directly is related, in some more or less complicated way, to the ozone distribution. Deriving the ozone distribution from the measurement involves the numerical solution of the equations expressing this relationship by a process generally known as "retrieval." The error analysis of the retrieval algorithm is an important part of evaluating the performance of the overall observing system.

The total ozone measurements made by the Dobson spectrophotometer and the Total Ozone Mapping Spectrometer (TOMS) and Solar Backscatter Ultraviolet (SBUV) instruments on Nimbus–7 are relatively simply related to the total ozone, so that the retrieval error analysis is straightforward. However, the profile measurements made by instruments such as the SBUV are very indirect. In some cases, the retrieval problem is "ill-posed" and needs a great deal of care.

We note that because the measurements are indirect, data from different observing systems will have different characteristics; this must be taken into account when comparing data from different sources. Consequently, the primary aim of this chapter is to characterise the algorithms that have been used for production processing by the major suppliers of ozone data to show quantitatively:

- How the retrieved profile is related to the actual profile. This characterises the altitude range and vertical resolution of the data.
- The nature of systematic errors in the retrieved profiles, including their vertical structure and relation to uncertain instrumental parameters.
- How trends in the real ozone are reflected in trends in the retrieved ozone profile.
- How trends in other quantities (both instrumental and atmospheric) might appear as trends in the ozone profile.

Error analyses for the ozone data that we have considered have, in general, been published in the open literature. Unfortunately, they have not been performed in a uniform and comparable way. We therefore decided to define a uniform error analysis and to apply it to all the data sources. At the request of the Ozone Trends Panel, these error analyses have been carried out by the experimenters.

Because it may be possible to largely eliminate random error in the long-term averages required for trends, retrieval methods appropriate to trend estimation are not necessarily the same as those appropriate to estimation of single profiles. However, the retrieval methods used for the data now available are designed for single profiles. It has become clear in the course of this study that data from some sources would be improved by reprocessing with improved methods; some data suppliers (e.g., Umkehr) are planning to do this. As our primary task is not to discuss the efficacy of the inverse methods used, but to characterise the ozone trend information currently available, we only consider in detail the algorithms that have been used to produce these data. However, we will make suggestions about retrieval methods suitable for trend estimation.

3.1 PROFILE RETRIEVAL CONCEPTS

The relationship between the ozone distribution and the quantity measured by a remote-sounding instrument is usually complicated and difficult to solve explicitly. The experimenters providing ozone data have used a wide range of retrieval methods to deal with the problem. In this section, we survey the types of methods used, as a background for our error analysis.

Any retrieval method uses some mathematical or numerical model of the relationship between the unknown profile and the quantity measured. We denote the quantities measured by an instrument in relation to any one profile by a vector $\mathbf{y}$, and the unknown ozone profile by a vector $\mathbf{x}$, which could be, for example, the mixing ratio at a set of altitudes. We describe the measurement algebraically or algorithmically by a *forward model* or *measurement model*, $F(\mathbf{x})$. The retrieval method will adjust the retrieved profile in some way so that the computed measurement corresponding to the retrieval agrees to some extent with the actual measurement. We describe this process by an *inverse model*, $I(\mathbf{y})$. Three classes of retrieval method have been used to produce the data studied here: onion peeling, relaxation, and linearisation with constraints.

The problem is fundamentally ill posed because the profile will always have structure on a scale finer than that on which it is possible to measure. Thus, all methods must use some explicit or implicit constraint on the solution. This usually takes the form of a profile representation that has finite vertical resolution.

A limb sounder measures a quantity that depends on the ozone profile only above the tangent height. If the profile is determined sequentially, starting at the top, then to find the ozone amount in the next layer down, it is only necessary to find the amount that matches the measured radiance (or transmittance, etc.) from that layer. Thus, onion peeling needs only to be able to solve a sequence of one-dimensional problems.

Relaxation methods solve the problem at all levels simultaneously by adjusting the profile according to a relaxation equation to improve the match between the measurement and the quantity computed by the forward model. The version of the Chahine method developed by Twomey et al. (1977) uses the following relaxation equation:

$$x_i^{n+1} = x_i^n \left[1 + \tilde{K}_{ij}(\mathbf{x}^n) \left(\frac{y_j^m}{F_j(\mathbf{x}^n)} - 1 \right) \right] \tag{1}$$

where n is an iteration index, i is a height index, $\tilde{K}$ is the weighting function (defined by Equation 2 below) normalised so that its maximum value is unity, and y_j^m is the measurement in channel j. The iteration is carried out for each channel in turn (i.e., for each j), and then repeated until convergence. The iteration modifies the profile in the region where the weighting function is nonzero by an amount that depends on the ratio of the measurement to the forward model.

If the forward model is linearised about some standard profile $\mathbf{x}_0$,

$$\mathbf{y} = F(\mathbf{x}_0) + \mathbf{K}_0(\mathbf{x} - \mathbf{x}_0) + O(\mathbf{x} - \mathbf{x}_0)^2 \tag{2}$$

where $\mathbf{K}_0$ is the Fréchet derivative $\partial F(\mathbf{x})/\partial \mathbf{x}$ evaluated at $\mathbf{x}_0$, then a Newtonian iteration can be used. Unfortunately, this relationship is usually ill posed; i.e., $\mathbf{x}$ has more elements than $\mathbf{y}$, so further constraints are required on $\mathbf{x}$. If we use a quadratic form constraint, and jointly minimise $(\mathbf{x}-\mathbf{x}_0)^T\mathbf{S}_x(\mathbf{x}-\mathbf{x}_0)$ and $(\mathbf{y}_l(\mathbf{x})-\mathbf{y}_m)^T\mathbf{S}_y(\mathbf{y}_l(\mathbf{x})-\mathbf{y}_m)$, where the matrices $\mathbf{S}$ express the nature of

the constant, y_l is the linearised forward model, and $\mathbf{y}_m$ is the measurement, then the iteration is of the form:

$$\mathbf{x}_{n+1} = \mathbf{x}_0 + \mathbf{S}_x\mathbf{K}_n^T(\mathbf{K}_n\mathbf{S}_x\mathbf{K}_n^T + \mathbf{S}_y)^{-1}[\mathbf{y}_m - F(\mathbf{x}_n) - \mathbf{K}_n(\mathbf{x}_0 - \mathbf{x}_n)] \quad (3)$$

Both the Twomey (1963) "minimum information" method and the optimal estimation approach reviewed by Rodgers (1976) are of this kind, with different interpretations for the constraint matrices.

3.2. ERROR ANALYSIS CONCEPTS

Many sources contribute to errors in retrieved ozone data sets. Those that lead to constant offsets or purely random errors are of minor importance when studying trends, as random errors will average out in the long run, and constant offsets make no difference to the trend. There are sources of error that distort the profile in some way, for example, by smoothing it. These are important because the derived trend profile will be similarly distorted. The most important sources of error are those that have trends themselves, which might appear as false trends in ozone.

To understand the nature of the retrieved data, we have carried out a formal error analysis of each observing system, including the instrument and the retrieval method. This will tell us how the retrieved data are related to the true profile and how the various sources of uncertainty affect the result. The error analysis must be general enough to apply to a wide variety of systems and to deal with various kinds of systematic errors. We generalise the forward and inverse model definitions to include some other parameters. The forward model becomes:

$$\mathbf{y} = F(\mathbf{x},\mathbf{b}) + \epsilon_y \quad (4)$$

The vector $\mathbf{b}$ represents any other parameters that the measurement might depend on, such as instrumental calibration or atmospheric temperature, and that may affect the derived ozone profile if not perfectly known. It may also be used to describe forward model deficiencies. The vector ϵ_y is the direct measurement error in $\mathbf{y}$. Note that, in principle, the measurement vector is in units of volts or telemetry counts, and not in scientific units. Calibration and retrieval are usually treated as separate processes operationally, but the boundary between them is often ill defined; they must be considered together for the error analysis.

The retrieved profile $\hat{\mathbf{x}}$ is related to the measurement in a way described by a slightly generalised inverse model:

$$\hat{\mathbf{x}} = I(\mathbf{y},\mathbf{b},\mathbf{c}) \quad (5)$$

where $\mathbf{c}$ represents any quantities that are used in the inverse model and subject to error or variability, but that do not appear in the forward model. The primary example is an a priori profile and its covariance, or an instrumental noise covariance assumed for the retrieval.

We can now formally relate the retrieved profile to the true profile. To carry out an error analysis with respect to the uncertain quantities $\mathbf{b}$, $\mathbf{c}$, and $\mathbf{y}$,

$$\begin{aligned}\hat{\mathbf{x}} &= I(F(\mathbf{x},\mathbf{b}) + \epsilon_y, \mathbf{b} + \epsilon_b, \mathbf{c} + \epsilon_c) \\ &= I(F(\mathbf{x},\mathbf{b}) + \epsilon_y, \hat{\mathbf{b}}, \hat{\mathbf{c}})\end{aligned} \quad (6)$$

where $\hat{\mathbf{b}}$ and $\hat{\mathbf{c}}$ are our best estimates of these parameters, but include errors ϵ_b and ϵ_c. This can be expressed in the form $\hat{\mathbf{x}} = T(\mathbf{x}, \mathbf{b}, \mathbf{c}) +$ *error terms*, where T is a *transfer function* relating $\mathbf{x}$ to $\hat{\mathbf{x}}$. Characterising the transfer function is one way of understanding how the retrieved profile is related to the true profile.

For the error analysis, we linearise about some ensemble mean $\bar{\mathbf{x}}$ and our best estimate of the forward model parameters, $\hat{\mathbf{b}}$ and $\hat{\mathbf{c}}$. We cannot use the true values of the model parameters, as they are not known.

$$\begin{aligned}\hat{\mathbf{x}} &= T(\bar{\mathbf{x}},\hat{\mathbf{b}},\hat{\mathbf{c}}) + \frac{\partial T}{\partial \mathbf{x}}(\mathbf{x}-\bar{\mathbf{x}}) + \frac{\partial T}{\partial \mathbf{b}}\epsilon_b + \frac{\partial I}{\partial \mathbf{c}}\epsilon_c + \frac{\partial I}{\partial \mathbf{y}}\epsilon_y \\ &= T(\bar{\mathbf{x}},\hat{\mathbf{b}},\hat{\mathbf{c}}) + \mathbf{A}(\mathbf{x}-\bar{\mathbf{x}}) + \mathbf{A}_b\epsilon_b + \mathbf{A}_c\epsilon_c + \mathbf{D}_y\epsilon_y\end{aligned} \tag{7}$$

thus defining the matrices $\mathbf{A}$, $\mathbf{A_b}$, $\mathbf{A_c}$, and $\mathbf{D_y}$. The first term is the transfer function operating on the ensemble mean $\bar{\mathbf{x}}$. Ideally, we might expect this to yield $\bar{\mathbf{x}}$, i.e.,

$$T(\bar{\mathbf{x}},\hat{\mathbf{b}},\hat{\mathbf{c}}) = \bar{\mathbf{x}} \tag{8}$$

but this is not necessarily true for the general retrieval algorithm. Any difference contributes to systematic error in the observing system.

The term $\mathbf{A}(\mathbf{x}-\bar{\mathbf{x}})$ is equivalent to the integral in a relation of the form

$$\hat{x}(z) = \bar{x}(z) + \int A(z,z')[x(z') - \bar{x}(z')]dz' + \text{other terms} \tag{9}$$

Thus, the rows of matrix $\mathbf{A}$ show how the observing system smooths the profile. Ideally, $\mathbf{A}$ would be the unit matrix $\mathbf{I}$, but in practise it is not, nor is it symmetric. We call the rows the *averaging kernels*. In regions where the retrieval is valid, they will be peaked functions centered on the appropriate altitude, having approximately unit area. They indicate the altitude range over which the observing system is sensitive to changes in the actual profile and give an indication of its vertical resolution. As an alternative to thinking of the averaging kernels' smoothing effect on the profile, we can consider the error in the solution contributed by structure on the vertical profile that is orthogonal to the averaging kernels. This is called the *null space* error. However, its size can be estimated only if the statistical behaviour of the true profile is known.

The columns of $\mathbf{A}$ differ from the rows and show the response of the retrieval to a δ-function perturbation in $\mathbf{x}$. Insofar as the linear expansion for $\mathbf{A}$ is valid, trends derived from retrieved data will have the same vertical resolution and range of validity as individual profiles.

Sensitivity of the observing system to forward model parameter errors is expressed by $\mathbf{A}_b$, and contributes to both systematic and random error, according to the nature of the errors in $\mathbf{b}$. Sensitivity to inverse model parameters is likewise given by $\mathbf{A}_c$. $\mathbf{D}_y$ expresses the sensitivity to instrumental noise. For the analysis of trends, the effect of the instrumental noise terms and the random components of the error in $\mathbf{b}$ is reduced by averaging. The important terms are the systematic errors in $\mathbf{b}$ and $\mathbf{c}$, especially those components that may have unrecognised, or unmodeled, trends themselves.

A full description of this approach to profile retrieval error analysis is being prepared for publication (Rodgers, 1988).

3.3 RETRIEVAL ANALYSIS FOR INDIVIDUAL INSTRUMENTS

In the following sections, we discuss the characteristics of the data supplied by instruments with a relatively long-term data record. These include SBUV, TOMS, Dobson, Stratospheric Aerosol and Gas Experiment (SAGE) –I and –II, the Solar Mesospheric Explorer (SME) Ultraviolet Spectrometer (UVS), and Near Infrared Spectrometer (NIRS). The Limb Infrared Monitor of the Stratosphere (LIMS) has been included as a source of validation data. The TIROS–N Operational Vertical Sounder (TOVS) has not been included, as the retrieval is by regression against Dobson measurements and it will have nothing of its own to say about trends.

We present a brief description of the forward and inverse models for each data source, and graphically display the averaging kernels and the major components of the systematic error. These diagnostics are used to assess the effect of the retrieval on the estimation of trends and the aliassing of trends in other quantities into apparent trends in ozone. Errors are 1σ, unless otherwise stated. For detailed descriptions of the instruments, see Chapter 2 of this report.

3.3.1 TOMS and SBUV Total Ozone

The TOMS instrument on Nimbus–7 consists of a monochromator whose narrow (3° × 3°) field of view (FOV) is scanned through the subsatellite point in a plane perpendicular to the orbital plane. Backscattered radiation is sampled at the six wavelengths—313, 318, 331, 340, 360, and 380 nm—sequentially in 3-degree steps in a ±51 degree cross-scan from the nadir. This scanning creates a contiguous mapping of the total ozone, since the scans of consecutive orbits overlap.

All TOMS data currently available from the archives (National Space Science Data Center—NSSDC) have been reprocessed using a new algorithm (Version 5) that uses a revised set of ozone absorption cross-section and instrument calibration parameters. The reprocessing started in December 1986 and was completed in July 1987.

The SBUV instrument (see Section 3.3.3) on Nimbus–7 measures total ozone by the same method, with a larger field of view (11.3 degrees square), and without the cross-track scanning. The wavelengths used for total ozone are 340, 331, 318, and 313 nm, a subset of the TOMS wavelengths. Both instruments are calibrated by viewing solar radiation reflected by the same diffuser plate, but with slightly different geometries.

3.3.1.1 Forward Model

The forward model used for analysis of the TOMS and SBUV data expresses the diffuse reflection of solar radiation by a multiple-scattering/absorbing atmosphere, bounded at the bottom by a diffusely reflecting surface. The physical basis of this forward model has been discussed by Dave and Mateer (1967) and reviewed subsequently by Klenk et al. (1982). The observational approach uses measurements at wavelengths near the long-wavelength end of the Hartley–Huggins O_3 absorption band. The wavelengths are chosen so that most of the radiance reaching the satellite instrument has passed through the ozone layer and has been backscattered from within the troposphere.

The absorption optical thicknesses for typical amounts of stratospheric ozone at the wavelengths used for ozone determination range from 0.05 to 0.5. The Rayleigh-scattering optical thicknesses for the entire atmosphere at these same wavelengths are around unity; about 90

percent of the scattering occurs in the troposphere. Thus, the backscattered radiance at the satellite depends on (1) the attenuation of the direct solar beam on its slant path through the ozone layer; (2) the reflecting power of the troposphere (molecular and aerosol scattering and surface and cloud reflections), and (3) the attenuation of the diffusely reflected radiation as it passes upward through the ozone layer.

If $\mu 0$ is the cosine of the Sun's zenith angle for the solar ray incident on Earth's surface at the view point, and μ is the cosine of the zenith angle of the line of sight to the satellite at the view point, then the total attenuation path of backscattered photons through the ozone layer, from (1) and (3), is approximately proportional to $1/\mu_0 + 1/\mu$. This proportionality is modified by the effects of the sphericity of Earth (important when μ or μ_0 are small) and by the presence of ozone in the tropospheric scattering layer.

An important aspect of the evaluation method is the treatment of cloud and surface reflections and backscattering by tropospheric aerosols. It is assumed that the average of these effects, over the instantaneous field of view, is that the atmosphere acts as if there were a Lambertian surface with equivalent albedo or reflectivity R. For a given wavelength, the forward model may then be written:

$$I(\Omega,\mu,\mu_0,R) = I(\Omega,\mu,\mu_0,0) + T(\Omega\mu,\mu_0)\ \frac{R}{[1 - RS(\Omega)]} \qquad (10)$$

where Ω is the total ozone, $I(\Omega, \mu, \mu_0,R)$ is the measured backscattered radiance, $I(\Omega, \mu, \mu_0,0)$ is the Rayleigh backscattered radiance from the atmosphere alone, $T(\Omega, \mu, \mu_0)$ is the direct plus diffuse radiance reaching the surface times the transmittance of the atmosphere for radiation reflected isotropically by the surface, and $S(\Omega)$ is the albedo of the atmosphere seen from below by the reflected surface radiance.

Precomputed tables of I, T, and S are used to evaluate the terms of the forward model. These data cover the full range of possible solar zenith angles and view angles. All orders of molecular scattering are accounted for by successive iteration of the auxiliary equation (Dave, 1964) in a pseudospherical atmosphere (DeLuisi and Mateer, 1971). The computations were carried out for 17 standard O_3 profiles, including 3 for a latitude of 15°, 7 for 45°, and 7 for 75°. Two sets of tables were computed: one for a surface pressure of 1.0 atm, the other for 0.4 atm. The ozone absorption coefficients are based on the measurements of Bass and Paur (1985). The effect of atmospheric temperature on ozone cross-sections is accounted for by using the three standard temperature profiles, one for each latitude. The computation of the band-averaged coefficients is described by Klenk (1980).

3.3.1.2 The Inverse Method

The surface albedo R is determined from the radiance measurements at 360 nm and 380 nm for TOMS and at 340 nm for SBUV, using Equation 10. All of these are outside the ozone absorption band, for which the Ω dependence drops out. This determination is dependent on tabulated values for $I(\mu, \mu_0,0)$, $T(\mu, \mu_0)$, and S. It is assumed that R is independent of wavelength.

Total ozone is inferred from the relative logarithmic attenuation N for absorbing wavelength pairs (λ_1, λ_2). The quantity N is related to the observations through the equation

$$N(\lambda_1, \lambda_2) = 100 \times [\log_{10}(I/F_0)_2 - \log_{10}(I/F_0)_1] \qquad (11)$$

where F_0 is the solar irradiance and I the measured backscattered Earth radiance, each at the wavelengths indicated. In the ideal case of a nonscattering atmosphere bounded by a Lambertian reflector, this quantity would be proportional to the total ozone in the optical path. When scattering is present, the relationship is nonlinear, and depends on the angles, the surface reflectivity, and the vertical distribution of ozone.

For TOMS, there are 12 separate estimates of total ozone: 4 from each of the 3 pairs—the A-pair (313/331), the B-pair (318/331), and the C-pair (331/340); for each pair from the two pressure tables (1.0 and 0.4 atm); and for each pressure from the two sets of standard ozone profiles from the latitudes nearest to the measurement latitude. The total ozone is linearly interpolated in latitude, except that between 0° and 15° latitude, only the 15° profile set is used, and polewards of 75°, the 75° profile set is used.

To combine the ozone values from the two pressures, an estimate is made of the effective surface pressure using the following procedure:

$$\bar{p} = wp_t + (1-w)p_c \tag{12}$$

where p_t is the terrain pressure, p_c is the estimated cloud-top pressure, and w varies from 0 to 1 based on surface reflectivity. It is unity for $R \leq 0.2$, zero for $R \geq 0.6$, and linearly interpolated for intermediate reflectivity. The cloud-top pressure is estimated in two ways: based on an empirically derived relationship that gives the cloud-top height as a function of latitude, and on an estimate based on the collocated infrared measurements from the THIR (temperature humidity infrared) sensor on Nimbus–7. The relationships used are "tuned" so that, on average, both estimates give the same total ozone amount.

The above rule is modified when snow or ice is known to be present (based on daily snow/ice maps from the U.S. Air Force). In such cases, it is assumed that there is only a 50 percent probability that clouds are present, despite the higher reflectivity, and the surface pressure ($\bar{p}$) derived above is averaged with the terrain pressure.

Finally, the three estimates of total ozone from the three pairs are combined using a weighting scheme that takes into account the varying sensitivities of the three pairs (with total ozone, solar zenith angle, view angle, and reflectivity) to total ozone amount and to errors in the retrieval. The combined estimate is reported as "best ozone."

3.3.1.3 Forward Model Assessment

The forward model scattering atmosphere is assumed to be Rayleigh; the lower boundary reflecting surface is assumed to be opaque and Lambertian. Simulation results (Dave, 1978) show that this assumption works well for aerosol optical thickness up to 1.0 except in unusual scattering situations, such as when two layers of thick clouds, separated by several kilometers of absorbing atmosphere, may be present.

The effects of the sphericity of Earth are accounted for only in the direct-beam and first-order scattering, but not in multiple scattering. The error in total ozone caused by this uncertainty is likely to be small.

Absorption by volcanic SO_2 has not been included in the forward model and the retrieval. This can clearly be seen as a perturbation in the retrieved total ozone for a short period after major eruptions, but it is quickly converted to H_2SO_4, and is unimportant for long-term studies.

3.3.1.4 Inverse Model Assessment

The primary source of error in deriving total ozone from the TOMS and SBUV measurements is the presence of tropospheric ozone. In the presence of thick clouds, the instruments obviously cannot measure the ozone column below the cloud layer. In effect, the algorithm adds an amount based on climatology. For a typical dark reflecting surface, even in the absence of clouds, variations in the total ozone column caused by changes in the ozone near the surface have relatively little effect on the measurement, because some backscattering takes place above this ozone. Therefore, effects of such variations will be underestimated in the TOMS- and SBUV-derived total ozone. A detailed discussion of this effect is given by Klenk et al. (1982).

Another possible source of error is the assumption that the surface reflectivity is wavelength independent. The TOMS instrument was designed with three reflectivity wavelengths (380, 360, and 340 nm) that can be used to study any possible wavelength dependence of the reflectivity. Early studies indicated no systematic wavelength dependence over different surfaces; therefore, the algorithm was designed to use a simple average of 380 nm and 360 nm reflectivities, whilst in the case of the SBUV, only 340 nm is used.

3.3.1.5 Error Analysis

Sensitivity to Diffuser Plate Reflectivity

The wavelength dependence of the sensitivity of retrieved total ozone to diffuser plate reflectivity D_λ is given in Table 3.1 for both TOMS and SBUV. On the basis of the discussion of diffuser plates in Chapter 2, we have carried out several tests (a–e, below) of the sensitivity of the retrieved total ozone to possible variations of diffuser plate reflectivity.

Table 3.1 Sensitivity of Retrieved Total Ozone to Diffuser Plate Reflectivity, $d \ln \Omega / d \ln D_\lambda$, for TOMS at Two View Angles, θ, and for SBUV. The Reference Atmosphere Contains 280 Dobson Units (DU) of Ozone, Surface Reflectivity is 0.3, and the Solar Zenith Angle is 45°.

λ (nm)	TOMS, $\theta = 0°$	TOMS, $\theta = 51°$	SBUV
313	0.71	0.53	0.58
318	0.71	0.62	0.72
331	−1.41	−0.85	−1.3
340	0.0	−0.34	0.24
360	0.13	0.11	—
380	0.12	0.10	—

(a) A random error of 1 percent in D_λ, uncorrelated between wavelengths, but constant in time. This gives a contribution to the formal random error in the total ozone, but should have no effect on the measured trend. The root mean square (rms) caused by this error source is given in row (a) of Table 3.2.

(b) A constant error of 1 percent in D_λ at all wavelengths. Thus, a drift of 1 percent per year in the error in D_λ would lead to an annual drift in total ozone given by row (b) of Table 3.2.

(c) A random error of 2 percent in $r(\lambda)$, the formal uncertainty quoted in Chapter 2. This is assumed to be uncorrelated between wavelengths, but constant in time. It leads to a scale error proportional to exposure time, whose value is random with an rms value given by row (c) of Table 3.2 at $E = 761$ hours (the end of the data set, after 8 years of measurements).

(d) A constant error of 5 percent in $r(\lambda)$. Five percent is roughly the scatter of the values of r given in Chapter 2, Figure 2.10. Row (d) of Table 3.2 gives the percentage error in total ozone from this source after an exposure time $E = 761$ hours.

(e) We have also considered the alternate diffuser plate models M1, M2, and L of Chapter 2. The change that these make to the retrieved total ozone relative to the model assumed by the OPT at an exposure time of 761 hours is given in Table 3.2.

Table 3.2 Sensitivity of Retrieved Total Ozone to Diffuser Plate Model Error Scenarios. The Basic State Is as for Table 3.1. The Details of the Scenarios Are Discussed in the Text.

λ (nm)	TOMS, $\theta = 0°$	TOMS, $\theta = 51°$	SBUV
(a) D_λ ±1%	1.7	1.2	1.6
(b) D_λ +1%	0.3	0.2	0.2
(c) $r(\lambda)$ ±2%	0.8	0.6	0.7
(d) $r(\lambda)$ +5%	0.4	0.3	0.4
M1 after 8 yrs	4.5	3.3	4.8
M2 after 8 yrs	2.9	2.0	3.1
L after 8 yrs	−0.6	−0.8	−0.8

Averaging Kernel

The "total ozone" measured by TOMS and SBUV is not the true total. It can be described as a weighted mean of the ozone density profile, plus an a priori contribution to allow for the tropospheric ozone not seen. The weighting function is close to unity for layers above the scattering layer, and smaller for layers below. For the tropospheric layers, the value of the weight can vary from zero (for thick clouds with tops near the tropopause) to near unity (for cloud-free scenes with a brightly reflecting surface). Typical weights for SBUV measurements with a solar zenith angle of 45° are <15 mb: 1.06; 15–30mb: 1.00; 30–100mb: 0.97; surface–100mb (cloud free): 0.7; cloud top–100mb (opaque cloud): 1.1–1.3; cloud top–ground: 0.0. These weights are appropriate for solar zenith angles up to about 70°, but will decrease considerably at low levels closer to the terminator.

A nominal value of 0.6 may be used for determining the error in the long-term trend due to changes in the tropospheric ozone.

Sensitivity to Atmospheric Temperature

The sensitivity of total ozone to atmospheric temperature is relatively small. At a nominal ozone density weighted atmospheric temperature of −46°C, the sensitivities are A-pair: 0.16 %/K; B-pair: 0.14 %/K; C-pair: 0.2 %/K. Note that the C-pair is used only near the terminator. The temperature dependence becomes even smaller at temperatures below −65°C. Thus, a temperature change of around 6–7K would be needed to produce a fictitious ozone change of 1 percent.

3.3.1.6 Trend Estimation Assessment

The primary source of error in TOMS and SBUV total ozone is the relative drift of the calibration of the diffuser plate reflectivity over the 20 nm intervals between the wavelength pairs. The range of possible models of the time change of the reflectivity leads to a drift in TOMS and SBUV total ozone of between −4.8 percent and +0.8 percent over the period 1978 to 1986. This could account for a large fraction of the drift relative to the Dobson network, discussed in Chapter 4.

The ozonesonde data indicate that tropospheric ozone may be increasing by about 1 percent per year (Logan, 1985; Tiao et al., 1986). The contribution to the column trend would be around 0.1 percent per year; about half of this would not be seen by SBUV and TOMS because these instruments are not sensitive to lower tropospheric ozone, but all of it would be seen by the Dobson instrument.

Although 8½ years' worth of TOMS ozone data are currently available, the TOMS instrument has had problems with its chopper electronics since April 1984. The best current estimates (Fleig et al., 1986) are that the error in total ozone data due to this problem has both positive and negative signs, with no more than 10 matm-cm error in any single measurement, no more than 5 matm-cm in the zonal mean of any given day, and no significant effect in deriving long-term trends.

3.3.2 Dobson Ozone Spectrophotometer: Total Ozone

The basic references for the Dobson Ozone Spectrophotometer are the *Observers' Handbook* (Dobson, 1957a, hereinafter BR1) and the *Adjustment and Calibration Manual* (Dobson, 1957b, hereinafter BR2). The instrument is used to measure the relative logarithmic attenuation of two wavelengths in the Hartley–Huggins ozone bands, one strongly and one weakly absorbed by ozone. These measurements may be made in either the direct sun (DS) or zenith sky (clear blue, ZB; or cloudy, ZC) modes of observation.

In some countries, the measurements are processed centrally and in others, at the individual instrument sites, but in all cases according to the process described in BR1.

3.3.2.1 Forward Model

For DS observations, the forward model for the relative logarithmic attenuation for a wavelength pair may be derived trivially from Beer's Law as

$$\begin{aligned} N &= \log_{10}(I/F_0) - \log_{10}(I'/F'_0) \\ &= (\alpha - \alpha')\mu\Omega + (\beta - \beta')mp + (\delta - \delta')\mu_0 + C_0 \end{aligned} \tag{13}$$

where I, I' are the solar irradiances for the short and long wavelengths, respectively,
F_0, F'_0 are the extraterrestrial solar irradiances,
α,α' are the decadic ozone absorption coefficients, atm-cm^{-1},
μ is the relative slant path of the Sun's rays through the ozone layer, $\simeq \mu_0$ for small solar zenith angles,
μ_0 is the relative slant path of the Sun's rays through the aerosols, generally mostly tropospheric,

Ω is the total ozone amount (atm-cm),
β,β' are the decadic Rayleigh scattering coefficients, atm^{-1},
m is Bemporad's optical air mass,
p is the station pressure, atm,
δ,δ' are the decadic optical depths for atmospheric aerosol,
C_0 is a constant including some instrumental effects and the log-ratio of the extra-terrestrial solar fluxes.

There is no provision in the standard forward model for absorption by other atmospheric gases such as SO_2, which is the main interfering gas.

The standard DS total ozone observation recommended by the International Ozone Commission and adopted by WMO is for the AD double pair (A-pair: 305.5, 325.4 nm; D-pair: 317.6, 339.8 nm), for which the forward model becomes

$$N_{AD} = N_A - N_D = 1.388\mu\Omega + 0.012mp \tag{14}$$

where 1.388 is the decadic ozone absorption coefficient difference for the double pair and 0.012 is the decadic Rayleigh-scattering coefficient difference for the double pair.

It is assumed that $(\delta-\delta')_A - (\delta-\delta')_D \simeq 0$ for the double pair measurements. Observations may also be made on the BD and CD double pairs (B-pair: 318.8, 329.1 nm; C-pair: 311.45, 332.4 nm).

There is no forward model for ZB or ZC observations.

3.3.2.2 Inverse Method

The inverse method for the DS observation follows directly from the forward model for the AD double pair as

$$\Omega = \frac{N_{AD}}{1.388\mu} - 0.009\frac{mp}{\mu} \tag{15}$$

The inverse method for ZB and ZC observations is entirely empirical. It is embodied in so-called zenith sky charts, that are developed from near-simultaneous DS and ZB observations. For further details, see BR1.

3.3.2.3 Forward Model and Inverse Method Assessment

The forward model for the double pair neglects the relative attenuation by atmospheric aerosol scattering and by absorption of atmospheric gases other than ozone, primarily SO_2 (see Komhyr and Evans, 1980, for example). It can be shown by Mie-scattering calculations for reasonable aerosol size distributions that the aerosol error in AD/DS total ozone observations is extremely small (for example, less than 1 matm-cm for the maximum aerosol optical depth over Mauna Loa following the El Chichón eruption). For SO_2 interference in urban areas, AD/DS total ozone observations will be approximately l matm-cm too high for each matm-cm of SO_2 present.

The forward model parameters include the ozone absorption coefficients and the Rayleigh-scattering coefficients. These are discussed in Section 3.3.4 on Umkehr measurements.

For DS observations, the forward and inverse models are essentially the same. The empirical ZB sky charts must be derived empirically and will represent average conditions. Their main deficiencies stem from the effects of aerosols on observations and the effects of differences in the ozone profile (for the same total ozone) on the observations. For ZC observations, the optical effects of the clouds will introduce additional errors.

3.3.2.4 Error Analysis

Ozone Absorption and Rayleigh-Scattering Coefficients

Errors in the absorption coefficient difference produce a change of scale in the total ozone measurements. The present standard IOC/WMO absorption coefficients give total ozone values 3–4 percent higher than the Bass-Paur (1985) coefficients. Rayleigh-scattering coefficients in current use may be in error by 1–2 percent; this will produce an insignificant bias in double-pair total ozone observations.

Absorption by SO_2

Absorption by SO_2 will produce erroneously high values of total ozone, as noted earlier. According to Komhyr and Evans (1980), the AD pair coefficient is 2.13, so that 1 matm-cm of SO_2 would appear as $2.13/1.388 = 1.53$ matm-cm of O_3. Evans et al. (1980) give 1.06 for this ratio. There may be errors due to SO_2 as great as 20–30 matm-cm in extreme cases (Kerr, private communication).

Instrumental Effects

Instrumental effects that may affect the total ozone measurements include optical alignment errors and wedge calibration errors. It is convenient to include errors in C_0 in this group. Interstation comparisons, using TOMS as a transfer standard, suggest that the above-noted errors produce a 2–3 percent variation in total ozone over the network.

Temperature Dependence

The temperature dependence of the derived total ozone is 0.13 %/K for AD pair measurements. This is unlikely to be significant.

Zenith Sky Measurements

ZB and ZC total ozone measurements have considerably greater errors than the DS measurements because of the empiricism in the inverse model and because of cloud effects. Errors as large as 20 percent may occur in extreme cases (thick clouds). These errors are discussed in Chapter 4, Ground-Based Measurements of Ozone.

3.3.2.5 Trend Estimation Assessment

Instrumental calibration changes produce errors in total ozone trend estimates made from a single instrument. How these are reflected in errors in the trend seen by the network is discussed in Appendix 1, Statistical Issues, and in Chapter 4.

Absorption and scattering coefficient errors are constant and will, therefore, have no impact on trend estimation.

Local (urban or regional) trends in tropospheric ozone are not strictly errors in total ozone measurements, but may serve to confuse the determination of "global" trends of total ozone. Trends in tropospheric SO_2 in urban areas will also introduce spurious trends in total ozone.

Only measurements taken by the direct sun (DS) method should be used for trends studies.

3.3.3 Solar Backscatter Ultraviolet Spectrometer

The SBUV data from November 1978 to February 1987 have been archived with the NSSDC. Instrument problems have arisen such that data collected after that date may be unsuitable for trend analysis. SBUV–2 data will be processed with the same algorithms as SBUV data.

3.3.3.1 Forward Model

The SBUV measures solar radiation that has been Rayleigh scattered by the atmosphere into the zenith direction and partially absorbed by ozone in the process. Ignoring the algebraic complication of sphericity, the observed backscattered UV radiance I_{obs} is given by

$$I_{obs}(\lambda) = \frac{F_0(\lambda)\beta(\lambda)P(\theta)}{4\pi} \int_0^{p_s} \exp[-(1 + \sec\theta)(\alpha(\lambda,T)X(p) + \beta(\lambda)p)]dp + I_{msr}(\lambda) \quad (16)$$

where F_0 is the direct solar irradiance, β is the Rayleigh-scattering coefficient per atmosphere, $P(\theta)$ is the Rayleigh phase function at solar zenith angle θ, α is the ozone absorption coefficient, $X(p)$ is the integrated ozone amount from the top of the atmosphere down to pressure level p, p_s is the surface pressure, and I_{msr} is the contribution to the measured radiance from photons multiply scattered by the atmosphere and reflected by the surface.

The primary unknown is $X(p)$; all the other variables apart from F_0, in Equation 16 are known, in principle. F_0 is measured by periodically viewing a diffuser plate of known reflectance, illuminated by direct solar radiation. The accuracy of this measurement and the degradation of the diffuser plate are critical and are discussed in detail in Chapter 2. The natural vertical coordinate system for this problem is pressure, rather than height, so SBUV measures ozone amount as a function of pressure.

The profile retrieval is carried out in terms of the quantity

$$Q_j = \frac{4\pi[I(\lambda_j) - I_{msr}(\lambda_j)]}{F_0(\lambda_j)\beta(\lambda_j)P(\theta)} \quad (17)$$

i.e., the integral in Equation 16. The penetration of solar UV radiation is primarily governed by the strength of the ozone absorption, which varies with wavelength. The Q-value has the dimensions of pressure, and in strongly absorbing regions (shorter wavelengths) it can be thought of as the pressure in the atmosphere at which the optical depth between the Sun and the instrument via this scattering level is about unity. In weakly absorbing regions (longer wavelengths), the solar radiation is scattered mainly from below the ozone layer, so the albedo is essentially a transmittance measurement depending largely on total ozone.

At the shorter wavelengths, the expression for single scattering (the integral in Equation 16) is sufficient. However, as the radiation at longer wavelengths penetrates to deeper levels (below about 15–20 km), multiple scattering and surface reflection become important and must be accounted for. I_{msr} depends on wavelength, surface reflectivity (cloud, ground, water, or snow), solar zenith angle, and the ozone profile. Fortunately, Taylor et al. (1980) have shown that it depends primarily on total ozone amount, and relatively little on ozone profile shape. Tables of I_{msr} have been calculated using the method of iteration of the auxiliary equation of radiative transfer (Dave, 1964; Dave and Furukawa, 1966), where the primary scattering is calculated for a spherical atmosphere, and higher orders assume a flat atmosphere. I_{msr} is pretabulated in terms of total ozone amount and surface reflectivity.

3.3.3.2 The Inverse Method

The retrieval approach is based on the optimal statistical estimation method (Strand and Westwater, 1968) as formulated by Rodgers (1976).

Three Retrieval Stages

The atmosphere is divided into 12 layers, based on the Umkehr layers (see Table 3.3); the ozone amount x_i in each layer is sought. The retrieval is formulated in terms of a profile vector $\mathbf{x}$ with elements $\ln(x_i)$ because of the wide range of possible values of x_i and to avoid negative quantities. To give more closely spaced layers needed to evaluate the forward model, the logarithm of total ozone X_j above each level, i.e., $\ln(\Sigma_{i=j}^{12} x_i)$, is interpolated in $\ln p$ using a cubic spline. Details of the sublayers are given in the same table.

Table 3.3 Layer Numbers Used by SBUV and Umkehr Retrievals

Layer Number	Pressure Range	Approx Km.*	No. of SBUV Sublayers
1	1013–253	0–10	14
2	253–127	10–14.5	7
3	127–63.3	14.5–19	7
4	63.3–31.7	19–23.5	7
5	31.7–15.8	23.5–28	7
6	15.8–7.92	28–33	7
7	7.92–3.96	33–38.5	7
8	3.96–1.98	38.5–43	7
9	1.98–0.990	43–48	7
10	0.990–0.494	48–54	7
11	0.494–0.247	54–59	7
12	0.247–0.127	59–64	7
	0.127–0	64–∞	1

*Using a midlatitude equinox temperature profile.

In practise, the SBUV retrieval is carried out in three stages. First, the three or four longest wavelength channels (depending on the solar zenith angle) are used to derive total ozone X_1 and surface reflectivity R using the algorithm described in Section 3.3.1.

In the second stage, a linearisation point is derived using latitude, day of year, and total ozone X_1 as a guide. For layers 6 through 12, the ozone amount in layer k is given by an equation of the form

$$x_k^a = A_k + B_k cos\{2\pi/365(J - J_{0k})\} \tag{18}$$

For layers 1 through 3, x_k^a is given by a quadratic function of total ozone, with coefficients independent of latitude and date. The coefficients used are given in the *SBUV Users Guide.* Layers 4 and 5 are fitted by assuming that the total ozone X_k above the base of layer k is cubic through levels 3, 4, 6, and 7, where *level* number n corresponds to the base of *layer* number n.

The third stage of the retrieval uses optimal estimation. The measurement vector $\mathbf{y}$ consists of $\ln(Q_j)$ for each channel together with the total ozone estimate X_1 from stage one. The a priori is taken to be the same as the linearisation point determined in stage two, together with a covariance matrix $\mathbf{S}_x$, which is independent of time and place.

The forward model linearised about a vector $\mathbf{x}_n$ is

$$\mathbf{y} = Q(\mathbf{x}_n) + \frac{\partial Q}{\partial \mathbf{x}}(\mathbf{x} - \mathbf{x}_n) = \mathbf{y}_n + \mathbf{K}_n(\mathbf{x} - \mathbf{x}_n) \tag{19}$$

thus defining the weighting functions $\mathbf{K}_n$, which are obtained by numerically integrating the algebraic derivative of $\mathbf{Q}$ with respect to each of the x_i in turn. The linearisation of the forward model for the total ozone measurement (i.e., $X_1 = \Sigma_1^{12} x_i$) is trivial.

The iteration to obtain x_{n+1} from x_n is

$$\mathbf{x}_{n+1} = \mathbf{x}^a + \mathbf{S}_x\mathbf{K}_n^T[\mathbf{K}_n\mathbf{S}_x\mathbf{K}_n^T + \mathbf{S}_\epsilon]^{-1}[\mathbf{y} - \mathbf{y_n} - \mathbf{K}_n(\mathbf{x}^a - \mathbf{x}_n)] \tag{20}$$

starting with $x_1 = \mathbf{x}^a$. Convergence is determined by the size of $\mathbf{x}_{n+1} - \mathbf{x}_n$.

The term $Q_{msr} = 4\pi I_{msr}/F_0\beta P(\theta)$ in Equation 17 depends primarily on total ozone amount, surface (or cloud top) reflectivity and pressure, zenith angle, and wavelength. It is found from a lookup table, using the retrieved total ozone, reflectivity, and a surface pressure estimated in the same way as for the TOMS and SBUV total ozone measurement (Section 3.3.1).

A Priori Assumptions

The a priori profile/linearisation point $\mathbf{x}^a$, used in the estimation equation, has a complicated history. The antecedent a priori profiles used in the original BUV algorithm (Bhartia et al., 1981) were based on a statistical analysis of ozonesonde data (Hilsenrath et al., 1977; Mateer et al., 1980) at levels below about 20 mb; the BUV observations at 274 and 283 nm were used to derive an exponential form for the profile at levels well above the mixing ratio maximum. The "upper" and "lower" profiles were joined by a cubic spline.

A priori profiles for the original processing of SBUV data were based on the World Ozone Data Center ozonesonde data archives for layers 1 through 5, and on the original BUV data set for layers 6 through 12. The profiles were fitted to an equation of the form

$$x_k^a = A_k + [1 - \cos(2\theta)][B_k + C_k \cos\{2\pi/365(J - J_{0k})\}] \tag{21}$$

where k is a layer index, θ is latitude, J is day of year, and A_k, B_k, C_k, and J_{0k} are regression coefficients.

The a priori profiles for the current SBUV algorithm (Bhartia et al., 1985) use the total ozone to estimate the layer 1, 2, and 3 amounts, using a quadratic relationship based on soundings at Natal, Brazil (5.9°S); Hohenpeissenberg, FRG (47.8°N); Churchill, Canada (58.8°N); and Resolute, Canada (74.7°N). For layers 6 through 12, the original processing of SBUV was fitted to an equation of the form of Equation 18.

The a priori profile error covariance matrix, $\mathbf{S}_x$, was developed for layers 1 through 5 as the covariance of the Hohenpeissenberg data set about the fitted values. The same process was used for layers 6 through 12 using the original SBUV data set, but with the subjective modifications to allow for the difference between the covariance of an ensemble of real profiles and that of an ensemble of retrieved profiles. Off-diagonal elements linking the two sets of layers were estimated subjectively. The same matrix is used for all latitudes and seasons.

Measurement Error Covariance

The measurement error $\mathbf{S}_\epsilon$ for stage three includes not only the errors in the measured radiance (0.5 percent) and total ozone (1.5 percent), but also the errors that enter into the calculation of y_n in Equation 19 and the calculation of the multiple-scattering correction. Thus, allowance is made for contributions to the measurement error covariance from errors in ozone absorption coefficients due to atmospheric temperature variations (0.5 percent). Surface reflectivity and surface pressure errors are not accounted for, but are believed to be small.

3.3.3.3 Forward Model Assessment

Single-Scattering Model

The method of calculating single scattering is considered to be highly precise for a molecular atmosphere because the coefficient for scattering by molecules is known to be better than 1 percent, and ozone absorption is believed to be 1 percent relatively and better than 2 percent absolutely. We have found no serious deficiencies in the integral in Equation 16.

Multiple-Scattering Corrections

The method used for calculating the multiple-scattering contribution involves the iteration of the auxiliary equation of radiative transfer in a pseudospherical atmosphere, in which only the primary scattered source photons for multiple scattering are calculated for a spherical-shell atmosphere. Higher order scattering is calculated for a flat atmosphere. This is considered to be a "reasonably good approximation" for SBUV out to a solar zenith angle of 88°, which is the maximum processed by the algorithm. The accuracy of this has not been checked, and we recommend that it should be. However, there should be no impact on trend estimates.

The lookup tables used for estimating I_{msr} are calculated from standard profiles; this approach is reasonable when I_{msr} is not a large correction. The error covariance matrix includes terms caused by the error in looking up the tables, but there is no numerical estimate of the accuracy of the parameterisation itself, particularly the dependence on the ozone profile.

Aerosols and Other Trace Gases

The effects of aerosol scattering and absorption, absorption by molecules other than ozone, fluorescence (both resonance and Raman), and scattering by other atmospheric gases are omitted in the forward model.

Fluorescence from nitric oxide has been detected in the continuous scan data from the SBUV (McPeters, 1986, 1989). Indeed, the decision not to use the 255 nm wavelength in the profiling algorithm was made because of interference from a strong NO fluorescence band resulting from absorption of solar radiation near 200 nm. The observed fluorescence is small (<4 percent of the Rayleigh scattering at 255 nm for the strongest bands), and is probably smaller above 260 nm.

O_2 is another molecule that is observed to fluoresce above 250 nm because of excitation by wavelengths near 200 nm (in the Schumann Runge Bands). In addition, O_2 can resonantly scatter in the Herzberg Bands between 250 and 300 nm. The analysis of the continuous scan data from SBUV by McPeters and Bass (1982) shows no peaks above 260 nm, but the superposition of the many fluorescent and resonant peaks could produce a quasi-continuum above 260 nm. No estimate of this continuum has been made.

Effects of the UV-absorbing gases NO_2 and SO_2 have been examined as possible sources of error; they were found to be insignificant under most circumstances. An exception to this is SO_2 from volcanic eruptions, but these are infrequent and short-lived phenomena, after which the SO_2 is rapidly converted to nonabsorbing sulphate compounds that produce stratospheric aerosol.

Scattering by stratospheric aerosols causes an increase in the measured albedo for the SBUV profiling wavelengths. For a normal stratospheric aerosol profile, this albedo change is strongly wavelength dependent. Figure 3.1 is a SAGE–I average aerosol profile for 5°S latitude for

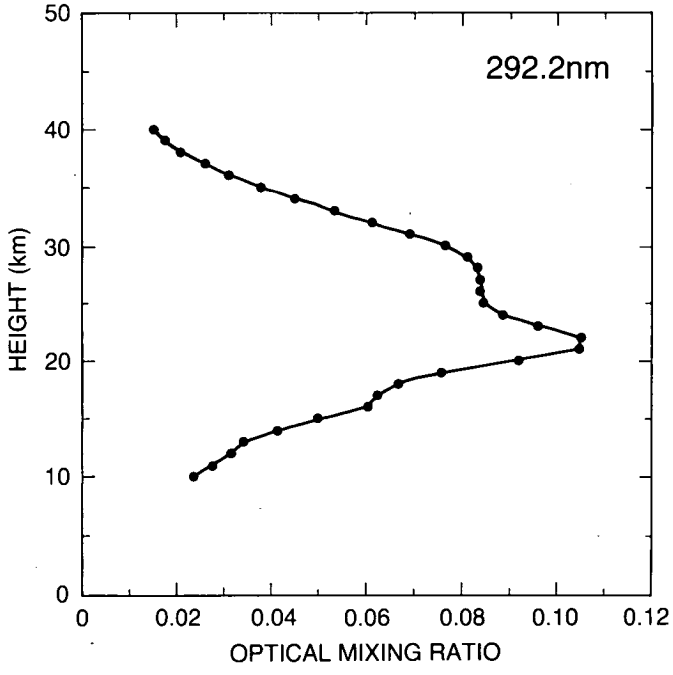

Figure 3.1. Aerosol profile from SAGE–I: average ratio of aerosol to Rayleigh extinction at 292 nm, for 5°S in summer 1980.

summer 1980, plotted as the scattering optical mixing ratio (aerosol extinction/Rayleigh extinction) as a function of altitude. The impact of this profile on the SBUV albedo is plotted in Figure 3.2 for the following case. The aerosol optical properties were defined by a real index of refraction of 1.435 and by taking the average of the properties for two size distributions of spherical Mie particles: modal radius 0.1 μm, standard deviation 0.4 μm, and modal radius 0.2 μm, standard deviation 0.4 μm. The calculations were made for a low-latitude ozone profile of 250 matm-cm, an effective surface reflectivity of 0.3, and a solar zenith angle of 0°. The SBUV albedo change has a rather sharp peak at 297.5 nm because the aerosol profile peak has a best match with the Rayleigh-scattering source function (or scattering layer) producing the backscattered albedo for this wavelength. The scattering layers for the other wavelengths are either above (λ<297.5) or below (λ>297.5), and the impact on these wavelengths is substantially reduced.

The effect of this albedo change "signature" on the retrieved profile is illustrated in Figure 3.3. Note the profile decrease in layers 6 and 7 and the increase in layers 5 and below. The reason for this decrease–increase pattern is that the total ozone is unaffected by these aerosols, so that the ozone removed from layers 6 and 7 has to be replaced because of the constraint that the retrieved profile should have approximately the measured total ozone.

This is only one example, intended to illustrate the impact of stratospheric aerosols on SBUV retrievals. In any particular case, the impact will depend on the aerosol optical properties (a function of index of refraction and aerosol size distribution) and on the aerosol profile. The effect will increase with aerosol amount; the retrieved profile distortion (level of the increase–decrease pattern) will depend on the aerosol profile shape (level of maximum optical mixing ratio).

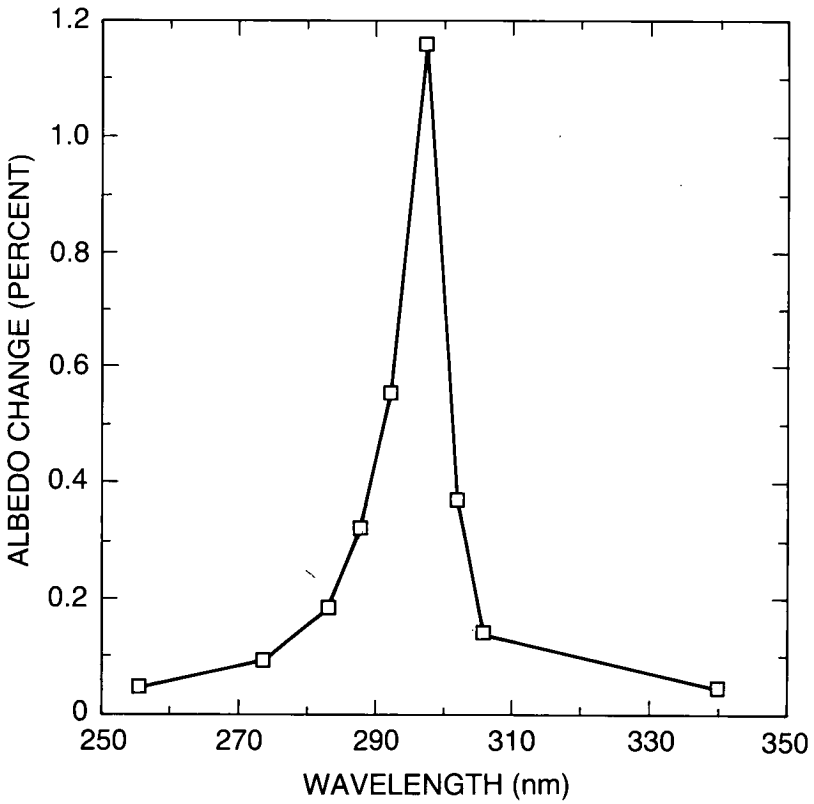

Figure 3.2. Calculated SBUV spectral signature for the Figure 3.1 aerosol profile. The assumed atmosphere contains 250 DU of ozone, the surface reflectivity is 0.3, and the solar zenith angle is 0°. Assumed aerosol optical properties are given in the text.

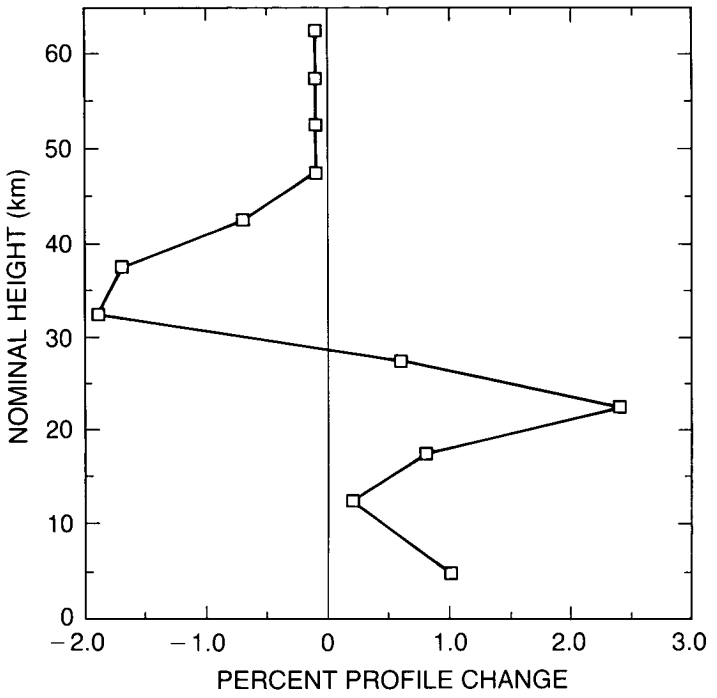

Figure 3.3. The effect of the Fig. 3.1 aerosol on the SBUV-retrieved ozone profile.

The climatology of aerosol optical properties and aerosol profiles is discussed in Chapter 10, on aerosols. Calculations using preliminary estimates of properties and profiles suggest that the large observed changes in SBUV albedo in the months immediately following the El Chichón eruption can be explained by calculations similar to those illustrated here.

Ozone Absorption and Rayleigh-Scattering Coefficients

The band-averaged ozone absorption coefficients for the SBUV wavelength bands are obtained using the procedure described by Klenk (1980), using Bass and Paur (1985) measurements of the ozone absorption spectrum in the ultraviolet and their reported temperature dependence.

For the computation of single-scatter radiances, the ozone absorption coefficients are computed at a nominal atmospheric temperature that varies with wavelength, determined by the altitude at which the weighting function peaks for that wavelength.

Since the atmospheric temperature effects are more important for the computation of I_{msr}, 3 standard temperature profiles are used, along with the 17 standard ozone profiles described in Section 3.3.1.1. The scattering coefficients are based on data from Bates (1984).

Instrument Attitude Errors

The instrument views the atmosphere nominally in the nadir direction. Any error in pointing knowledge will appear primarily as solar zenith angle errors. However, with a field of view of 11.3 degrees, the expected variations of spacecraft attitude of a few tenths of a degree will not seriously affect the measurement. No significant bias error is expected from attitude errors.

3.3.3.4 Inverse Method Assessment

We have found no significant problems with the inverse method. To the extent that the forward model is correct, the retrieval will reproduce the measurements within experimental error.

The constant a priori covariance used in the retrieval is based in part on the subjective modification of an earlier set of SBUV and BUV retrievals. As such, it may represent an ensemble of profiles that are too smooth at higher altitudes and, hence, constrain the retrieval too tightly.

The second-stage retrieval leads to difficulties in extreme situations, such as the Antarctic ozone hole (McPeters et al., 1986), where the algebraic forms described in Section 3.3.3.2 are used outside their region of validity, giving rise to unrealistic initial profiles that are reflected in the final retrieval. However, the error analysis below shows that the profiles are unsuitable for trend studies in this altitude range for other reasons.

Apart from the ozone hole problem, however, most of these comments are not of immediate significance for trend measurement as they do not introduce spurious trends and are taken into account in the retrieval characterisation presented in the next section.

3.3.3.5 Error Analysis

Forward model parameters include the absorption coefficient, α, the Rayleigh scattering coefficient, β, the diffuser plate reflectivity and its wavelength dependence, and the surface/cloud albedo and pressure. Inverse model parameters include the a priori regression coefficients and the a priori and measurement error covariances.

Averaging Kernels

The averaging kernels show how the retrieved ozone profile is related to the true profile. In an ideal observing system, the averaging kernel for *layer i* would be unity within *layer i* and zero outside. They have been computed for a range of cases, including midlatitude conditions with total ozone of 325 and 525 matm-cm, a low-latitude case, and a high-latitude case representative of the ozone hole.

Figure 3.4 shows the averaging kernels for a midlatitude case. These curves are partial derivatives $\partial \ln \hat{x} / \partial \ln x$ of the log of the retrieved layer amount, with respect to the log of each of the sublayer amounts.

We note that layers 6 to 9 or 10 give averaging kernels (ak's) centered at approximately the correct nominal level and with a full width at half maximum of about 1.6–2 Umkehr layers (8–10 km). The layer 10, 11, and 12 ak's are all centered on layer 10, with significant negative excursions at layer 8. The layer 5 ak is very broad, whilst the layer 1 to 4 ak's are generally peaked in the wrong place, have significant negative excursions, and are found to vary considerably from one case to the next.

We must conclude that only the retrievals from layer 6 to layers 9 or 10 are of value for trend estimation as they stand. Trends derived from layers 1 to 5, 11, and 12 may be misleading because the retrievals depend on the ozone variations at other levels. It may be that the retrievals for these layers are reasonable estimates of ozone in those layers on a single profile basis, but that

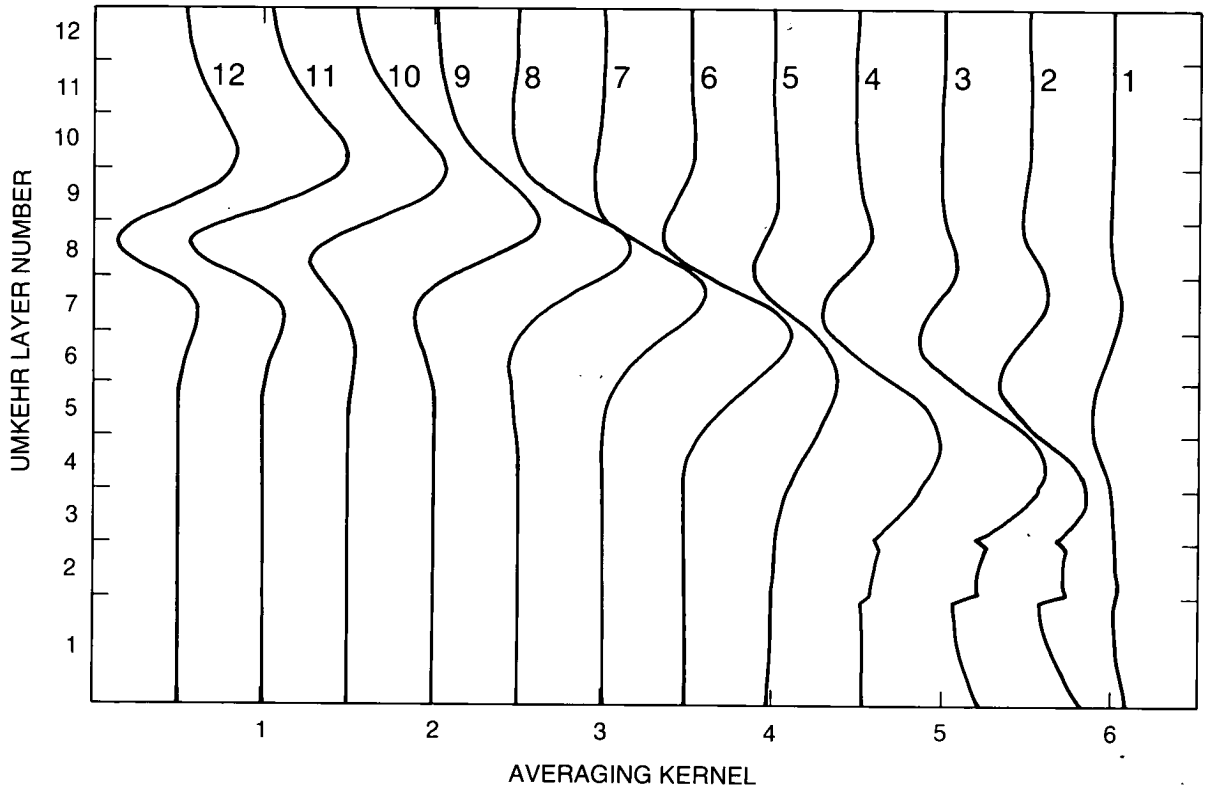

Figure 3.4. SBUV averaging kernels for retrieved layer amounts. The reference profile is at a midlatitude (45°), solar zenith angle is 45°, and a total ozone amount is 325 DU. The curves are labeled with layer numbers and offset by multiples of 0.5 for clarity.

is because there are correlations between levels in the ozone climatology. This is not appropriate for trend estimation, where past climatology of individual profiles may not be a good estimate of the climatology of future changes.

Sensitivity to Diffuser Plate Reflectivity

If the measured value of the diffuser plate reflectivity D_λ is in error by δD_λ, then the measured Q-value will be in error such that $\delta \ln(Q_\lambda) = \delta \ln(D_\lambda) = \delta D_\lambda / D_\lambda$. Thus, the sensitivity of the retrieved profile to diffuser plate errors is the same as its sensitivity to the measured Q-value. On the basis of the discussion of diffuser plates in Chapter 2, we have carried out several tests of the sensitivity of the retrieved profile to diffuser plate reflectivity:

(a) A random error of 1 percent in D_λ, uncorrelated between wavelengths, but constant in time. This gives a contribution to the formal random error in the profile, but should have no effect on the measured trend. The rms of this error source is curve (a) in Figure 3.5.

(b) A constant error of 1 percent in D_λ at all wavelengths. Thus a drift of 1 percent per year in the error in D_λ would lead to an annual drift in profile given by curve (b).

(c) A random error of 2 percent in $r(\lambda)$, the formal uncertainty quoted in Chapter 2. This is assumed to be uncorrelated between wavelengths, but constant in time. It leads to a scale error proportional to exposure time, whose value is random with an rms value given by curve (c) in Figure 3.5 for $E = 761$ hours (8 years).

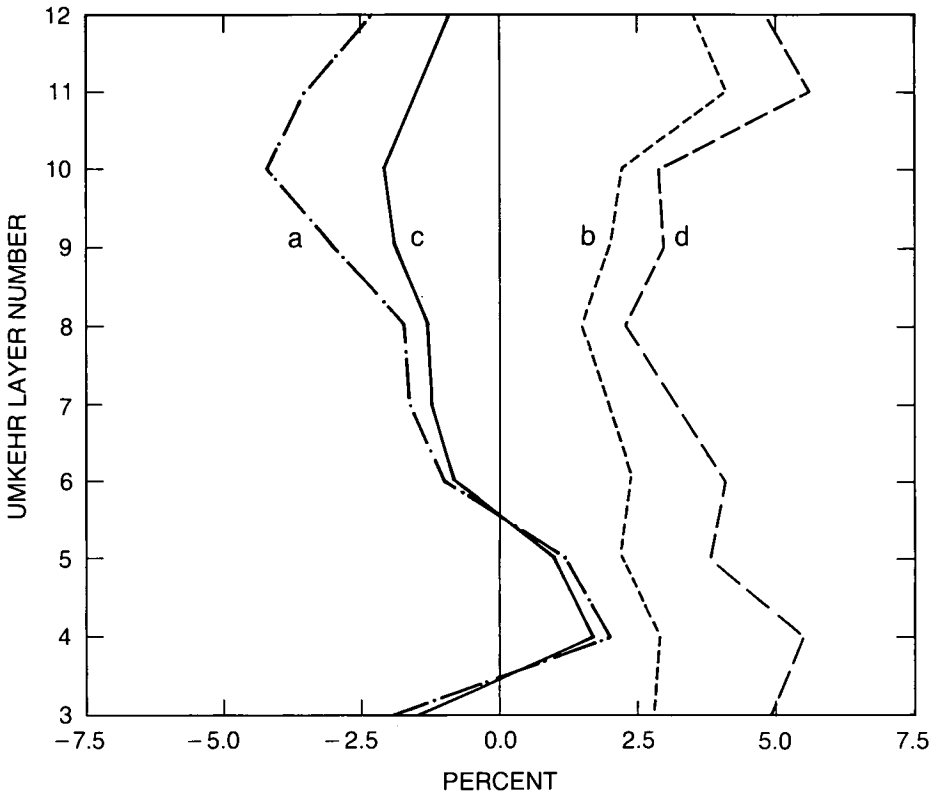

Figure 3.5. (a) rms error in the SBUV profile due to a 1 percent random error in D_λ. (b) increase in ozone due to an increase in D_λ of 1 percent at all wavelengths. (c) rms scale error due to a 2 percent random error in $r(\lambda)$, after 8 years' operation. (d) increase in ozone due to a 5 percent increase in $r(\lambda)$ at all wavelengths.

(d) A constant error of 5 percent in $r(\lambda)$. Five percent is roughly the scatter of the values of r given in Chapter 2, Figure 2.10. Curve (d) shows the effect of this error at $E = 761$ hours.

(e) We have also considered the alternate diffuser plate models M1, M2, and L of Chapter 2. The change that these make to a retrieved midlatitude profile is shown in Figure 3.6, for a profile measured at the end of the data set, after 8 years. The change here is so large that it is probably outside the bounds of this linear error analysis, but this should give a guide to the magnitude of the error.

Sensitivity to Atmospheric Temperature

The retrieved ozone profile will depend on atmospheric temperature through the temperature dependence of absorption coefficient. Figure 3.7 shows the percentage change in the retrieved profile to a temperature perturbation of 1K in each layer. We note that, to produce a 1 percent change in ozone at level 6, we would need about a 10K change in temperature in layers 6 and 7.

Sensitivity to Surface or Cloud Top Reflectivity and Pressure

The sensitivities of the profile to surface or cloud top reflectivity and pressure are shown in Figure 3.8. Except at levels 1 to 3, both are very small and are unlikely to be significant.

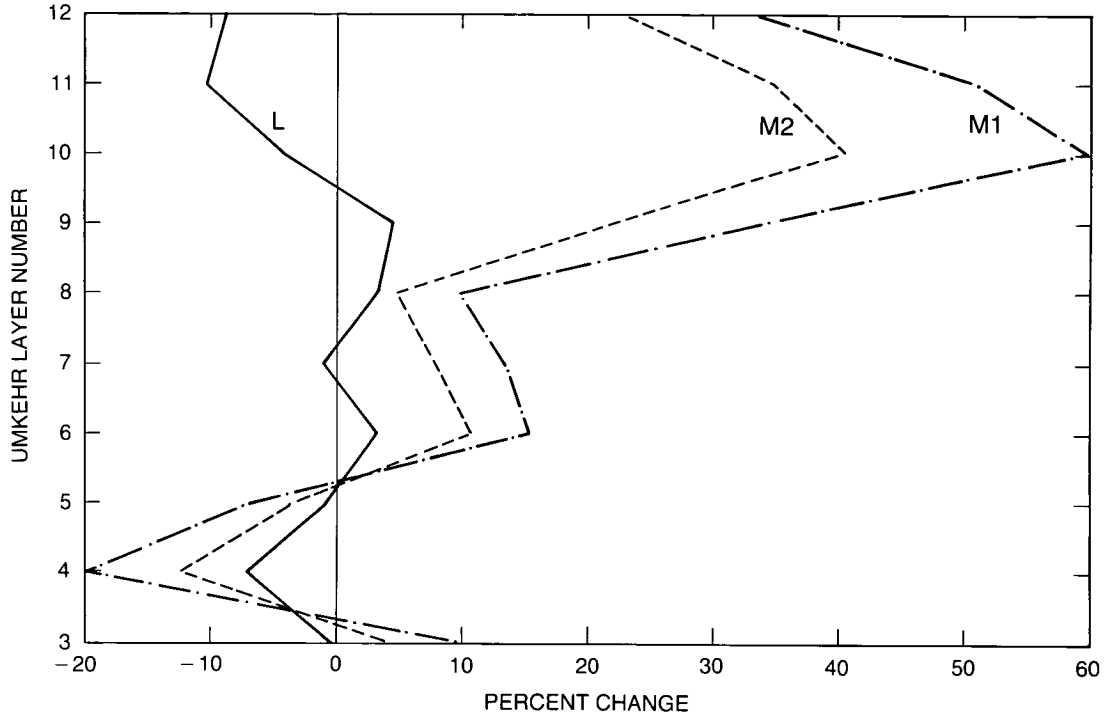

Figure 3.6. Change in ozone relative to the SBUV archived data, due to the diffuser degradation models M1, M2, and L, as defined in Chapter 2.

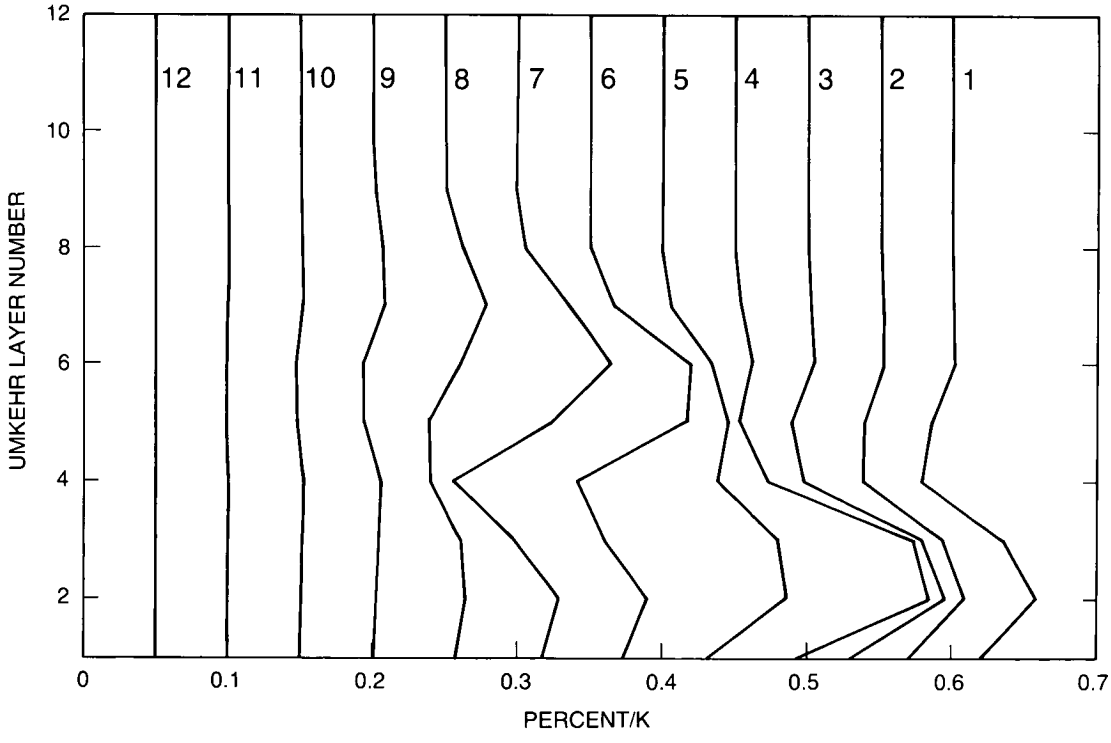

Figure 3.7. Sensitivity of the SBUV retrieved layer amounts to errors in the mean layer temperatures. The curves are labeled with the layer in which the temperature is perturbed and are offset by multiples of 0.05%/K for clarity.

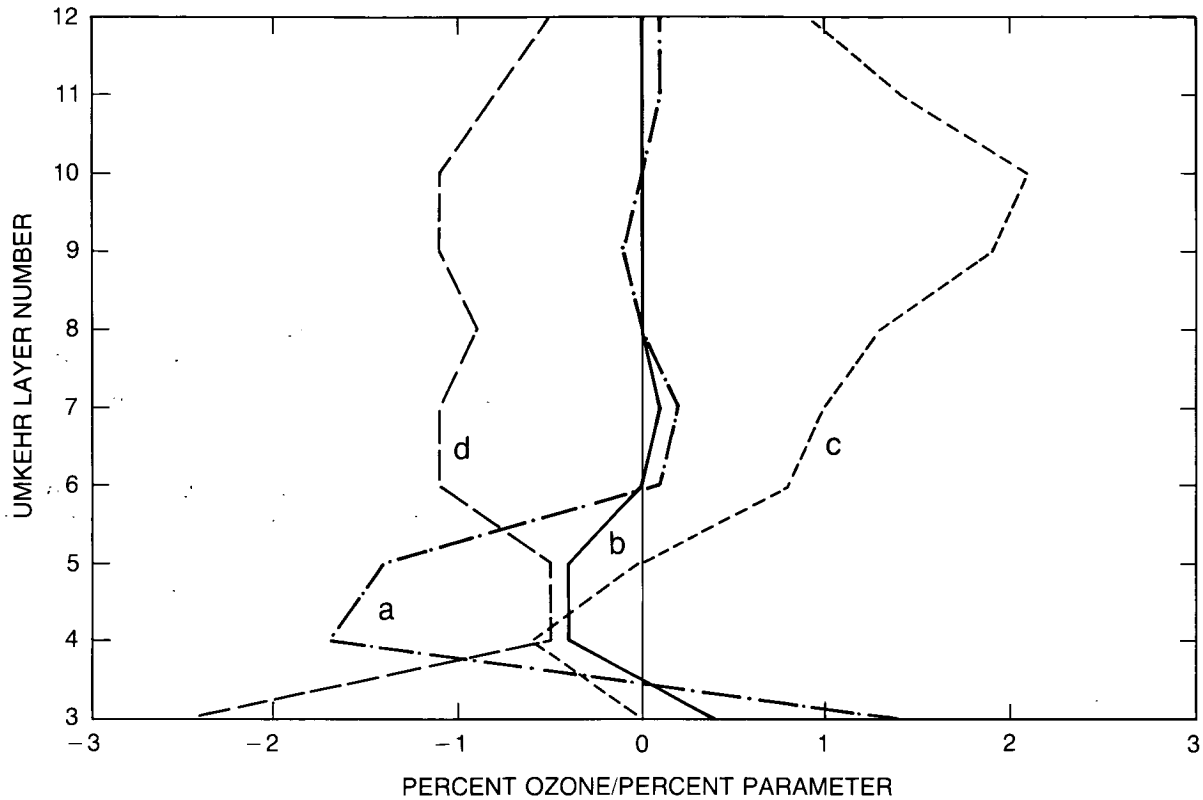

Figure 3.8. Sensitivities of the SBUV-retrieved layer amounts to errors in (a) surface reflectivity (b) surface pressure (c) Rayleigh-scattering coefficient (d) ozone absorption coefficient.

Sensitivity to Ozone Absorption and Rayleigh-Scattering Coefficients

The ozone absorption coefficients and Rayleigh-scattering coefficients, or their errors, will not change with time. Therefore, errors due to this cause will not contribute to trend errors. The sensitivities shown due to these causes are given in Figure 3.8 for completeness.

Sensitivity to Aerosol

A formal error analysis of the sensitivity to aerosol is complex, and has not been carried out by us. A case study giving a typical impact is discussed in Section 3.3.3.3 above; further discussion will be found in Chapter 10.

3.3.3.6 Trend Estimation Assessment

The averaging kernel plots indicate that SBUV data should be capable of representing the ozone profile between Umkehr layers 6 and 9 or 10 (16–0.7mb, 28–51 km) with a vertical resolution of 1.6–2 layers (8–10 km). Trends should be measurable in the same range with the same resolution, except insofar as they are aliased by trends in other quantities involved in the retrieval. The most important uncertainties, which may introduce unreal trends into the data, are diffuser plate reflectivity and atmospheric aerosol. Our best estimate of the diffuser plate uncertainty leads to the conclusion that the apparent trends in currently archived SBUV ozone profiles (Chapter 5) are not significantly different from zero, and that SBUV measurements are not capable of definitively identifying the ozone depletion due to chlorofluorocarbons (CFC's)

that is predicted by the chemical models (Chapter 7). This position may change if further information on the diffuser degradation becomes available. This does not, of course, apply to SBUV–2, for which an archival data set is not yet available.

Atmospheric temperature, as well as surface or cloud-top reflectivity and pressure, have the potential of introducing apparent trends, but these effects are small.

The problem with the second stage of the retrieval mentioned in (d) above implies that current SBUV profile data below about 20 km cannot be used for ozone hole studies. However, the averaging kernels analysis implies that the retrievals in that altitude range are dubious for other reasons.

3.3.4 Dobson Ozone Spectrophotometer: Umkehr

The Dobson spectrophotometer measures the ratio of zenith sky or direct Sun radiance at two wavelengths in the ultraviolet. An Umkehr observation consists of a series of zenith sky measurements taken as the solar zenith angle changes from 60° to 90°. The observation includes a concurrent measurement of the total ozone column with the same instrument (Section 3.3.2). In the standard technique, as reported in the World Ozone Data Center archives, the C-pair of wavelengths centered at 311.45 and 332.4 nm is used. The present standard algorithm, which is described and assessed in this section, was developed by Mateer and Dütsch (1964).

3.3.4.1 Forward Model

The solar radiation received by the instrument is scattered mainly by the gaseous atmosphere and absorbed mainly by ozone. The physics of the measurement is basically the same as that for SBUV (Section 3.3.3), but the geometry is different.

The forward model used in Umkehr retrieval accounts for scattering only by the gaseous atmosphere (assumed to obey the Rayleigh scattering law) and for absorption only by ozone. For this idealized atmosphere, computation of zenith sky light is relatively straightforward, although somewhat tedious, especially at solar zenith angles near 90°, where the effects of the sphericity of Earth need to be accounted for precisely. Since the scattering optical depth of the atmosphere at the Umkehr wavelengths is near unity, multiple-scattering effects are also important.

In the real atmosphere, there is also scattering by the dust and aerosols suspended in the atmosphere at different altitudes. Other gases, such as SO_2, are also sometimes present in sufficient quantities to provide significant absorption.

Determination of Ozone Absorption Coefficient

The Dobson instrument has a band-pass of about 1 nm at the shorter wavelength and close to 4 nm at the longer wavelength of the C-pair. Therefore, the instrument is sensitive to the radiation received in a range of wavelengths over which the scattering and absorption properties of the atmosphere may vary. For forward model calculations, however, it is convenient to assume that the instrument is sensitive to a pseudo-monochromatic radiation, having both an effective ozone absorption value and an effective scattering cross-section. The effective ozone cross-sections used in the standard Umkehr algorithm were obtained by convolving the meas-

urements of Vigroux (1953) (at −44°C) with the nominal instrument band-passes for each wavelength (for band-passes, see Vigroux, 1967). These cross-sections are published in the Dobson instrument manual (Dobson, 1957b).

Computation of N-Value Tables and Derivatives

The full forward model is too complicated for efficient use in standard retrievals, so it is approximated for this purpose by a set of second order Taylor series expansions of the full model about a set of three standard profiles.

The N-value tables and first-order partial derivatives used in the standard algorithm are calculated in a manner that accounts for the sphericity of Earth for the primary and second-order scattering. A flat-atmosphere multiple-scattering code was used to calculate the ratio of total multiple scattering to secondary scattering. Each spherical-shell secondary scattering radiance was then multiplied by the appropriate ratio to obtain an equivalent spherical-shell total multiple scattering. For the first-order partial derivatives, this same radiance ratio was used to obtain an equivalent spherical-shell multiple-scattering partial derivative. The calculation of the second-order partial derivatives involved only primary scattering in a spherical-shell atmosphere. The effects of atmospheric refraction were not included in these calculations.

3.3.4.2 The Inverse Method

The inverse method is based on the "minimum information" method of Twomey (1963).

$$N(\mathbf{x},\theta) = 100\log_{10}\left[\frac{I(\mathbf{x},\theta,\lambda_1)}{I(\mathbf{x},\theta,\lambda_2)}\right] + C_0 \tag{22}$$

where $\mathbf{x}$ is the profile to be estimated, θ is the solar zenith angle, $I(\mathbf{x},\theta,\lambda)$ is the zenith sky radiance at wavelength λ, and C_0 is the "extraterrestrial constant," a combination of the solar spectrum and the instrumental response. The measurement vector $\mathbf{y}$ comprises the Dobson total ozone X_{obs} and the quantities $N'(\mathbf{x},\theta_i)$, obtained by subtracting $N(\mathbf{x},60°)$ from each of the other N-values.

The elements of the profile vector $\mathbf{x}$ are $-\ln(x_i)$, where x_i is the ozone amount in Umkehr layer i.

The second-order expansion of the forward model is written

$$\mathbf{y} = \mathbf{y}_{std} + \mathbf{K}(\mathbf{x} - \mathbf{x}_{std}) + (\mathbf{x} - \mathbf{x}_{std})^T\mathbf{L}(\mathbf{x} - \mathbf{x}_{std}) \tag{23}$$

where $\mathbf{K}$ is the first-order derivative and $\mathbf{L}$ is the second-order derivative, both evaluated at $\mathbf{x}_{std}$. For the retrieval, the vector $\mathbf{u}$ is defined

$$\mathbf{u} = \mathbf{K}(\mathbf{x} - \mathbf{x}_{std}) = \mathbf{y} - \mathbf{y}_{std} - (\mathbf{x} - \mathbf{x}_{std})^T\mathbf{L}(\mathbf{x} - \mathbf{x}_{std}) \tag{24}$$

An ozone conservation equation is added to the set as the forward model for X_{obs}. The retrieval iteration is

$$\hat{\mathbf{x}}^n = \mathbf{x}_{std} + (\mathbf{K}^T\mathbf{K} + \gamma\mathbf{I})^{-1}\mathbf{K}^T\mathbf{u}^{n-1} + \gamma(\mathbf{x}_{fg} - \mathbf{x}_{std}) \tag{25}$$

where $\mathbf{x}^{n-1}$ is used in evaluating the quadratic term in $\mathbf{u}^{n-1}$, $\mathbf{x}_{fg}$ is a first-guess profile, and γ is

Twomey's smoothing constant. The convergence criterion is based on the change in size of the quadratic term between iterations.

Three standard profiles are used, each containing different amounts of total ozone. The linearisation point is chosen to be one of the three, on the basis of the total ozone amount. The first-guess profile is also chosen to be one of the standard profiles on the same basis, except that for total ozone amounts near the changeover points, a linear interpolation is used so that there are no discontinuities in the first guess as a function of total ozone. No seasonal or latitudinal variation is used in the standard profiles.

3.3.4.3 Forward Model Assessment

Ozone Absorption Coefficient Calculation

The spectral characteristics of the received radiation depend on the extraterrestrial spectrum, the solar zenith angle, the ozone profile, the temperature profile, and the scattering and absorbing constituents of the atmosphere. Consequently, strictly speaking, for a given effective ozone cross-section, agreement between calculated and "true" band-pass-averaged radiation can occur only for a limited range of conditions. Fortunately, simulation studies suggest that this error is less than 1 percent for a broad range of atmospheric conditions.

The algorithm is based on the assumption that all instruments in the Umkehr network have essentially the same band-pass. Actual instrument band-passes have been measured for only one instrument (Komhyr, unpublished), and these were generally broader than the nominal band-passes used by Dobson (1957a,b). However, interstation total ozone intercomparisons, using TOMS as a transfer standard, suggest that the standard error in total ozone measurements arising from both absorption coefficients (via band-pass and spectral alignment problems) and from extraterrestrial constant (C_0) errors combined does not exceed about 2 percent (Bojkov and Mateer, 1985; conclusion from data in their Table 1). This may be considered an indication of interstation precision.

Insofar as absolute errors in the effective absorption coefficients are concerned, Table 3.4 is relevant.

Table 3.4. Effective Ozone Absorption Coefficients for Dobson C-Pair

Source	T(°C)	Short	Long	Diff.	Ratio
[a]1. Dobson, 1957, Vigroux, 1953	−44	2.100	0.108	1.992	19.4
2. Vigroux, 1967	−50	1.957	0.099	1.858	19.8
[b]3. IOC–WMO, 1968	—	(1.941)	(0.099)	1.842	(19.6)
4. Bass & Paur, 1985	−45	2.0044	0.0917	1.9127	21.86
[c]5. Error Tests	—	1.9303	0.0883	1.842	21.86
% Range excl. (5)		8.2	17.8	8.1	12.7

[a]Standard Algorithm
[b]Effective 1/1/68
[c]Section 3.3.4.5

The absorption coefficient difference in line 3 was adopted by WMO in 1968 for use in total ozone measurements, but values were not specified for the individual wavelengths. The values in parentheses were estimated for use in the assessment of the sensitivity to errors in absorption coefficient and spectral alignment in Section 3.3.4.5. The values in line 1, used in the standard algorithm, are considerably in error, due at least in part to the spectral sparseness of the early Vigroux measurements. The Bass–Paur data are stated to have a precision of 1 percent between 245 and 330 nm. The precision at the long C wavelength is not this good—perhaps 2 percent. The absolute accuracy is related to the measurement of Hearn (1961) of the ozone cross-section at 253.65 nm, which is believed to be accurate to about 2–3 percent. The assumption in the standard algorithm of an isothermal atmosphere (−44°C) introduces distortion in the retrieved profiles, due to temperature dependence of the absorption coefficient.

Calculation of N-Value Tables and Derivatives

The quadrature for the spherical-shell part of the N-value and partial derivative calculations should be accurate to better than 0.5 percent for primary scattering and to 1 percent for secondary scattering. The quadrature for the flat-atmosphere multiple-scattering calculations should also be accurate to better than 1 percent. The extension of the flat atmosphere calculations to third and higher orders of scattering in a spherical atmosphere may lead to errors as great as 3 percent (estimated) in the radiance ratio (1.3 N-units) for a solar zenith angle of 90°, where the error is greatest. Errors in the first-order partial derivatives may be somewhat greater.

The application of the second-order partial derivatives, which are calculated for primary scattering only, involves some empirical adjustments developed by Dütsch (unpublished). This process should not involve significant errors for ozone profiles close to one of the standard profiles. Errors for profiles that are not close to one of the standard profiles have not been determined; they may be significant.

Aerosol and Other Scattering

The forward model used in the Umkehr retrieval does not account for the scattering by dust, aerosols, and thin clouds sometimes present during the measurement. The main reason for this is that the quantity of suspended matter is extremely variable from day to day, and its optical properties are rarely known accurately enough to include it correctly in the forward model. Consequently, the error introduced by aerosol scattering remains the most significant source of error in Umkehr retrievals over the short term, as well as in determining seasonal and long-term variations of ozone.

With the present-day theoretical capability of calculating radiative transfer for a molecular medium, including large-particle scatters, it is possible, in principle, to include aerosol effects directly into an Umkehr forward model. This would be valuable only if the aerosol properties were known a priori for each observation. However, the Umkehr inverse model is not capable of separating aerosol information from ozone information. Aerosol properties that must be known are phase function, albedo of single scattering, and vertical profile. It is not practical to measure these properties, which can be quite variable with time, at all Umkehr stations on a regular basis.

A detailed discussion of the effect of aerosols on Umkehr retrievals, and on possible approaches to making corrections, is found in Chapter 10.

Absorbers Other Than Ozone

The only known absorber of any significance that has been omitted from the forward model is SO_2, which may occur in highly polluted urban environments (see Section 3.3.2) and in the stratosphere as a short-lived species immediately after major volcanic eruptions.

3.3.4.4 Inverse Method Assessment

Accuracy of the Second-Order Expansion

The standard algorithm starts with a known linearisation-point profile and a precomputed table of *N*-values. As the estimated profile is modified during the iteration process, the table values are adjusted to account for the change. This adjustment is calculated using precomputed coefficients of a truncated (after second order) Taylor series expansion of the *N*-values around the a priori profile.

As discussed in Section 3.3.4.3, the calculation of these coefficients is not sufficiently accurate and may introduce error in the forward model calculation. The impact of error in the coefficients will be insignificant when the atmospheric ozone profile is close to the a priori, but could be significant when it is not.

Ozone Above Layer 9

The retrieval method solves for the ozone amount in layers 1 to 9. However, there is enough ozone above layer 9 to cause significant absorption of the strongly absorbing wavelength at large solar zenith angles. The Umkehr retrieval assumes an a priori value of 2.07 matm-cm above layer 9, and that this amount is always 54 percent of the layer 9 amount. These figures are derived primarily from photochemical calculations carried out in the early 1950's. Recent satellite and rocket measurements indicate that 2.07 is too large, by about 50 percent, and that the value varies seasonally.

3.3.4.5 Error Analysis

Averaging Kernels

Averaging kernels have been computed for a range of cases, showing how the retrieved layer ozone is related to the true ozone profile. In an ideal observing system, the averaging kernel for *layer i* would be constant within *layer i*, and zero elsewhere. Figure 3.9 shows that is by no means the case. Only one example is shown; the others gave results that were qualitatively similar but that differed in detail. A summary of the peak heights and widths of the averaging kernels is given in Table 3.5.

We note that, for layers 4 through 8, the averaging kernels are peaked at approximately the right level, with a full width at half maximum of around 2.5 layers. The kernels for layers 3 and 9 have significant negative excursions; they are peaked about one layer too high and low, respectively. The kernels for layers 1 and 2 are more complicated functions of the true profile; they appear to be unrelated to the ozone in those layers. The averaging kernel also describes the relationship between the measured trend profile and the true trend profile, so trends with a broad vertical structure between layers 4 and 8 would be reasonably well measured, but retrieved trends in layers 1, 2, 3, and 9 should be treated with caution.

Table 3.5. Averaging Kernel Peak Heights and Widths

Layer	Level of Maximum			Full Width Half Height	
	Layer	p(mb)	H (km)	Layers	H (km)
1	—	1013	0	2.4*	12
2	3.56	60.6	19.4	2.9	14.5
3	4.06	42.9	21.6	2.4	12
4	4.56	30.3	23.8	2.8	14
5	5.31	18.0	27.2	2.9	14.5
6	6.19	9.84	31.2	2.6	13
7	6.69	6.96	33.5	2.3	11.5
8	7.69	3.48	38.3	2.2	11
9	7.94	2.92	39.6	2.0	10

*One-sided

Absorption Coefficient and Spectral Alignment

Errors in the ozone absorption coefficients used in the algorithm have been discussed in Section 3.3.4.3. A spectral alignment problem may be considered equivalent to an absorption coefficient error for an individual instrument.

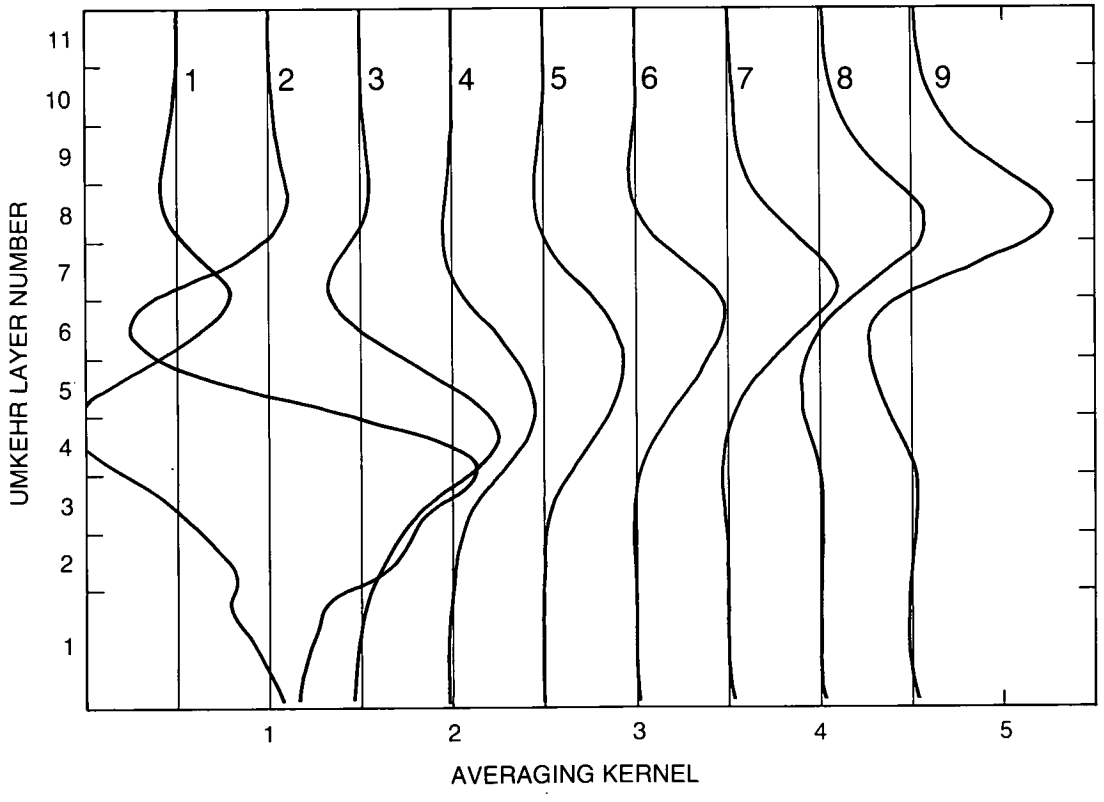

Figure 3.9. Umkehr averaging kernels for retrieved layer amounts. The reference profile is a midlatitude profile with a total ozone amount of 340 DU. The curves are labeled with layer number and offset by multiples of 0.5 for clarity.

Umkehr retrievals are sensitive to the difference in the absorption coefficients for the short- and long-wavelength channels and to their ratio. An error in the difference produces, primarily, an error in scale, accompanied by some profile distortion. An error in the ratio of the coefficients produces profile distortion in the retrievals. The sensitivity of the retrieval to errors in the coefficients for the individual channels is shown in Figure 3.10. This result has been obtained by perturbing the standard algorithm.

Additional results have been obtained using another algorithm in the following manner. First, the values in line 3 of Table 3.4 were used to obtain an average Umkehr retrieval for 20 Umkehr observations at Arosa (Switzerland) in 1980. Second, the values in line 5 were used to obtain an average retrieval for the same 20 Umkehrs. This retrieval, shown as a percentage difference from the first one in curve (a) of Figure 3.11, illustrates the effect of changing the coefficient ratio to the Bass–Paur value while holding the coefficient difference unchanged. This coefficient change produces very little profile change in layers 1 and 6, increases up to 1 percent in layers 2–5, and decreases as much as 4.5 percent above layer 6, i.e., a profile distortion. Curve (b) in Figure 3.11 is obtained using the Bass–Paur values in line 4 of the table. As noted above, comparing curve (b) with curve (a), this has produced primarily a scale change of between 3 and 4 percent, except in layer 1 where there is little change. Roughly similar results would apply if this procedure could be applied to the standard algorithm.

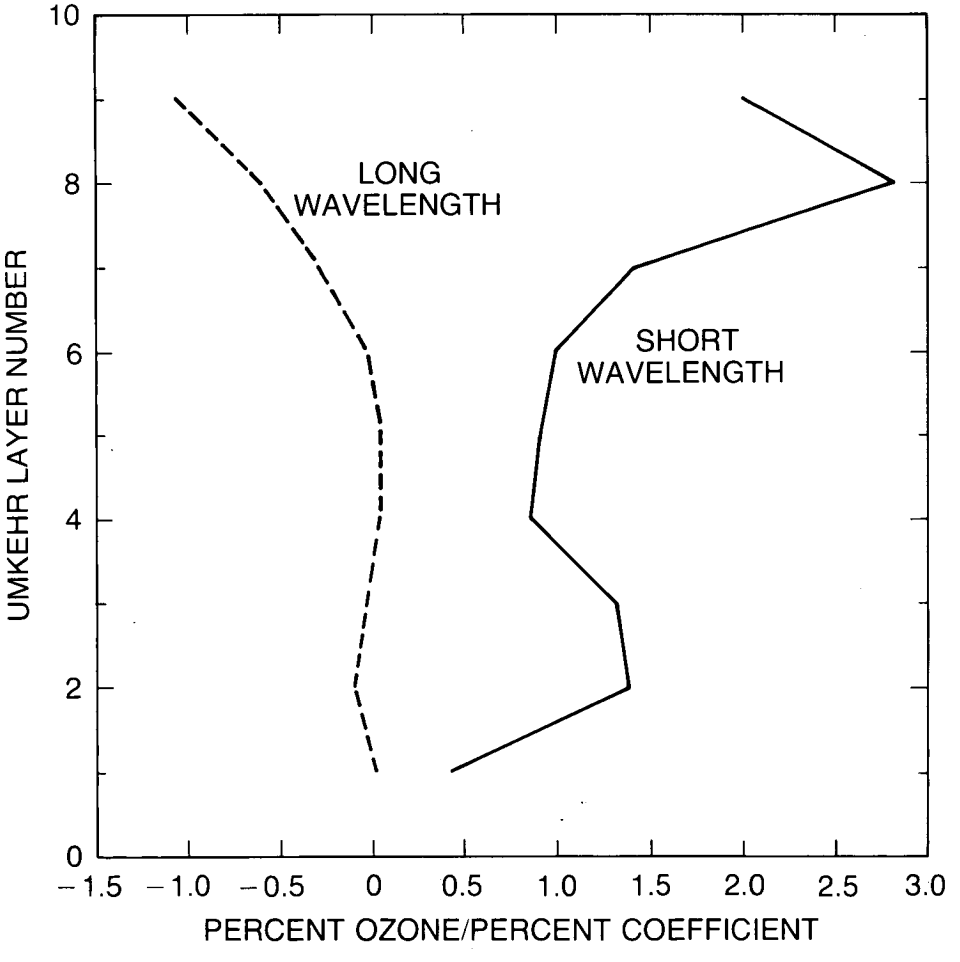

Figure 3.10. Sensitivity of the Umkehr retrieval to absorption coefficient errors.

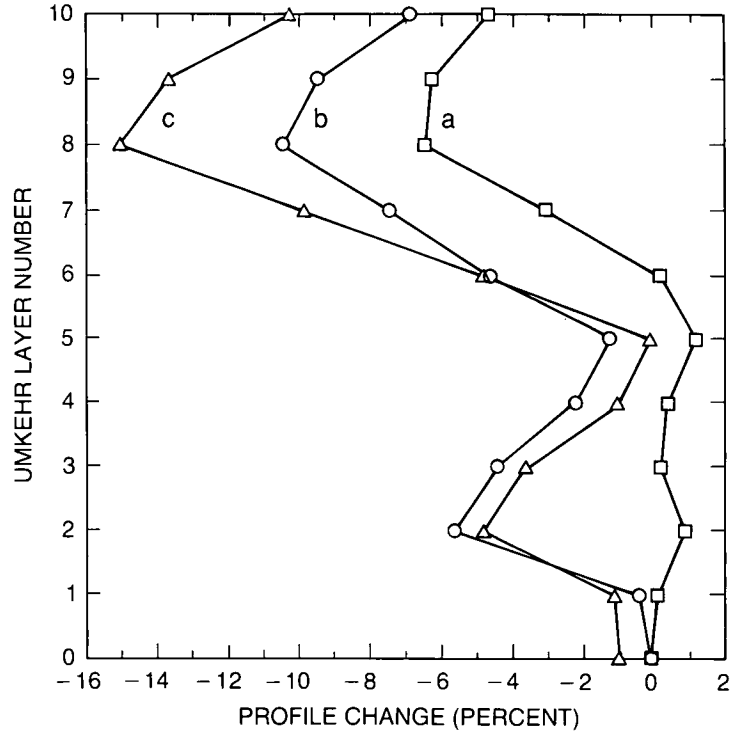

Figure 3.11. Changes in Umkehr retrievals due to the following absorption coefficient assumptions: (a) changing the coefficient ratio to the Bass–Paur value, keeping the difference unchanged. (b) Bass–Paur values at −44°C. (c) Bass–Paur values, including temperature dependence.

Finally, we must explain how the change in 1968 in the scale of C-pair total ozone has been handled in the standard algorithm. First, the observed total ozone value on the 1968 scale is multiplied by 0.925 (= 1.842/1.992) to reduce it to the scale implied by the coefficients used in the algorithm. The inversion is then carried out using the algorithm. Finally, all layer amounts in the retrieved profile are divided by 0.925 to convert them back to the 1968 ozone scale. This procedure introduces some profile distortion (similar to curve (b) minus curve (a) in Figure 3.11), but should have little effect on ozone trends derived from Umkehr profiles. Curve (b) alone gives an idea of the overall profile bias (distortion) caused by the use of the incorrect coefficients.

Temperature

Umkehr profile retrievals are also sensitive to atmospheric temperature through the temperature dependence of the ozone absorption coefficients. The short wavelength coefficient of the C-pair has a temperature sensitivity of 0.15%/K, while the long wavelength sensitivity is 0.37%/K. Failure to include this temperature dependence, as in the standard algorithm, which assumes a constant temperature of −44°C, produces an additional profile distortion. This distortion is such that atmospheric layers that are warmer than −44°C will have too much ozone in the retrieved profile, and vice versa. The result of adding the temperature dependence for an average midlatitude temperature profile is illustrated by comparing curve (c) with curve (b) (isothermal atmosphere at −44°C). The greatest effect is seen in the 40–50 km region, where the temperature is significantly warmer than −44°C.

It is evident that real temperature trends will introduce fictitious ozone trends in Umkehr profiles. Figure 3.12 illustrates the effect of a 20K temperature change in each layer. For this

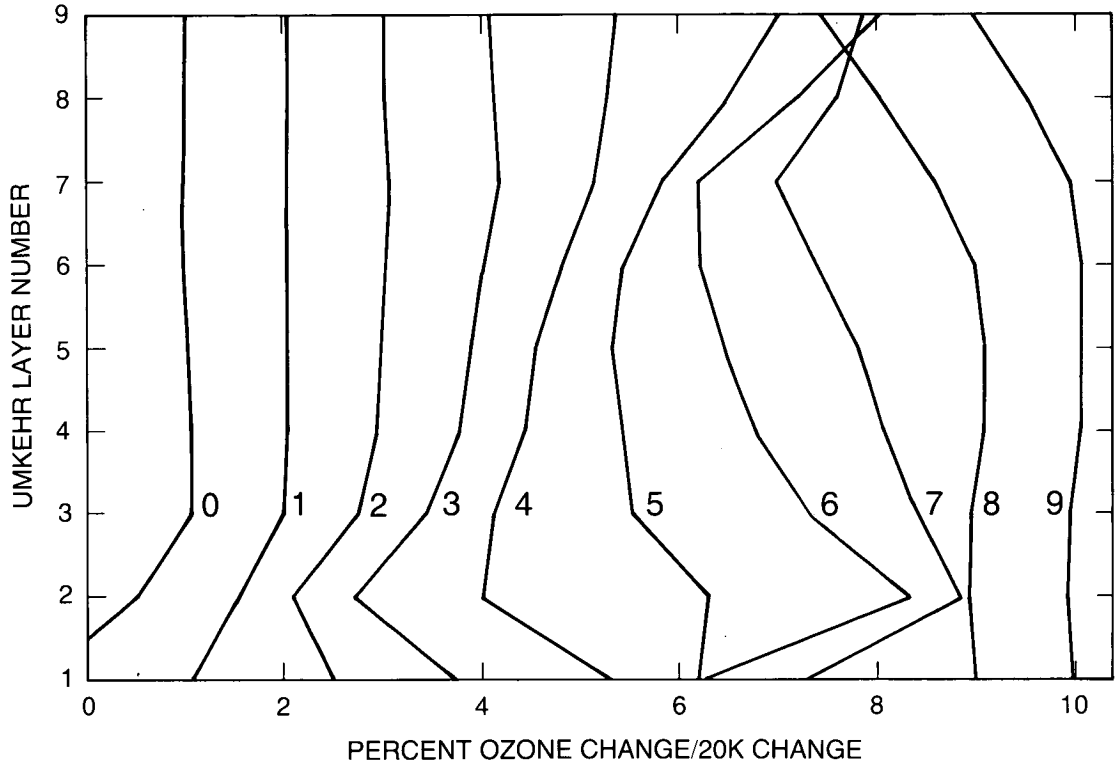

Figure 3.12. Sensitivity of Umkehr-retrieved ozone to atmospheric temperature changes. The curves are labeled with the number of the layer in which the temperature is perturbed by 20K and are offset by 1%/20K for clarity.

particular test, the troposphere (layer 1) has been divided into two layers (curves 0 and 1). We may conclude that realistic atmospheric temperature trends will have a rather small effect.

Rayleigh-Scattering Coefficients

The Rayleigh-scattering coefficients β are known to better than 1 percent. The change in the retrieved profile for a change in β of 1 percent is shown in Figure 3.13. This is a small but constant systematic error.

Total Ozone Measurement

An error in the extraterrestrial constant C_0 has no effect on the N-values, but affects the total ozone measurement. As noted in Section 3.3.4.3, this error combined with others does not exceed about 2 percent over the Dobson network. Sensitivity of the retrieved profile to the total ozone measurement is given in Figure 3.14. This sensitivity is small, except for layer 1.

Surface Reflectivity

The standard algorithm assumes zero surface reflectivity, whereas typical reflectivities might be around 20 percent, approaching 100 percent in the case of snow cover. Sensitivity to assumed surface reflectivity is given in Figure 3.15. The error in retrieved ozone is unlikely to be more than about 1 percent, except in layer 1. This is unlikely to contribute to errors in trends.

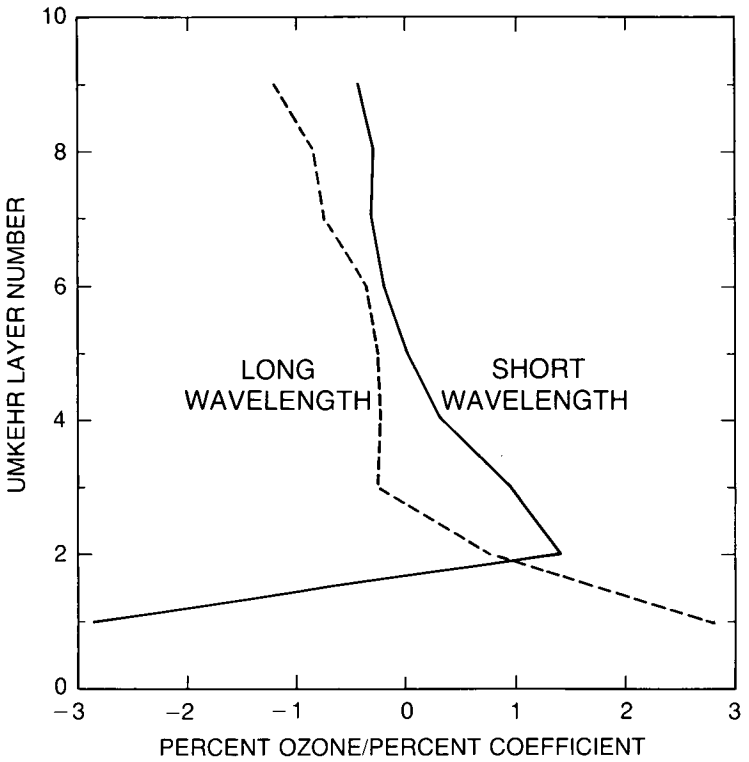

Figure 3.13. Sensitivity of Umkehr-retrieved ozone to Rayleigh-scattering coefficient errors.

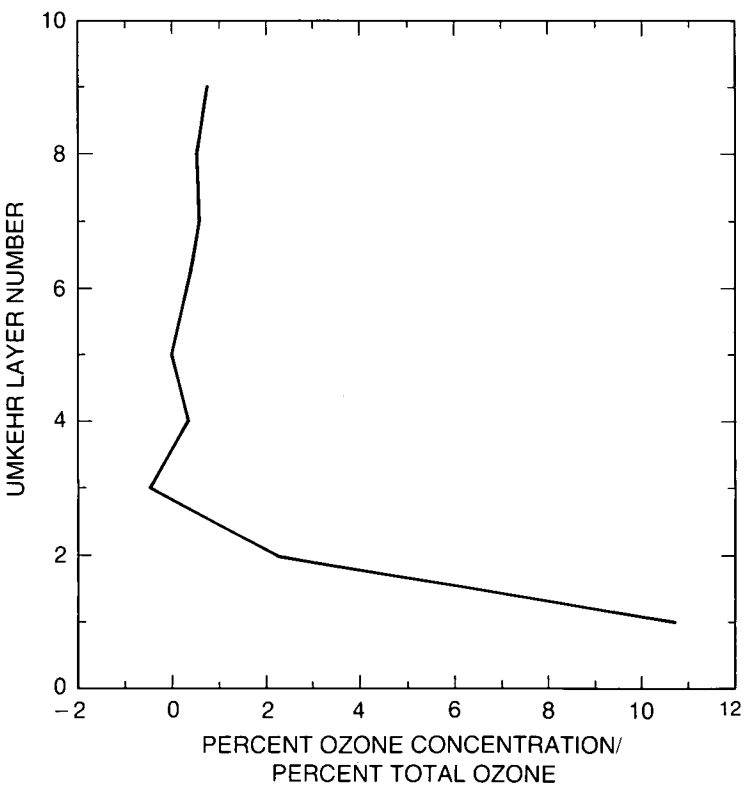

Figure 3.14. Sensitivity of the Umkehr-retrieved profile to errors in the total ozone measurement.

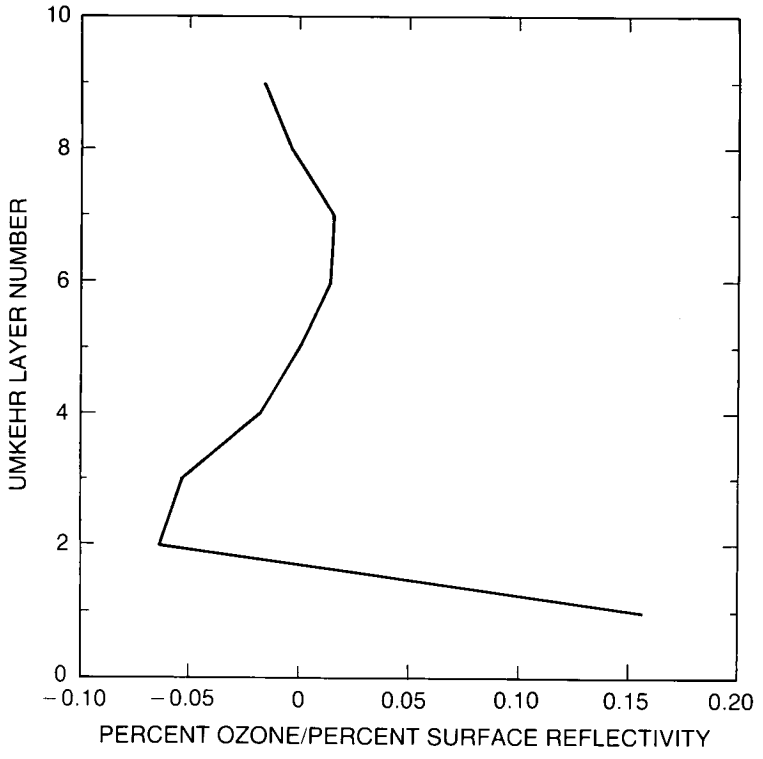

Figure 3.15. Sensitivity of the Umkehr-retrieved profile to surface reflectivity errors.

Multiple-Scattering Correction

The error in the multiple-scattering correction has not been determined. An estimate of this error has been obtained by computing the corrections, using the pseudospherical atmosphere method for one of the standard profiles, and taking the difference between these corrections and those used in the standard algorithm. The effect of this difference on the retrieved profile is shown in Figure 3.16. The profile changes are small for layer 4, with roughly a 5 percent increase for higher layers, and decreases below layer 4 with a maximum 20 percent decrease in layer 2. These errors should be primarily systematic and have little effect on trends.

Other Absorbers

The effect of unaccounted SO_2 absorption on the retrieved profile, for 1 matm-cm in the lower half of layer 1, corresponding to a typical background (i.e., low pollution level) urban troposphere (Kerr, private communication), is shown in Figure 3.17. Also shown is the effect of a moderately heavily polluted troposphere, with 10 matm-cm. This is significant for quality control, but should not be for trends, unless a significant number of stations are in polluted areas.

Volcanic SO_2 is very short lived and has not been considered here.

Other Effects

Wedge calibration and other similar discontinuities in the record may be corrected if the information is available (it has been done for Belsk, Poland). This has nothing to do with the

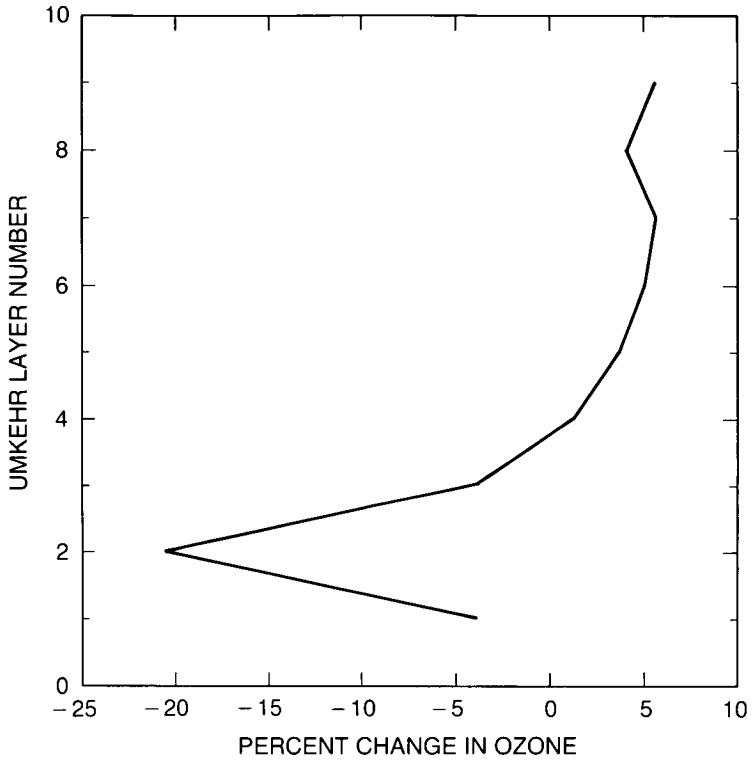

Figure 3.16. Effect on the ozone profile of changing the method of calculating the multiple-scattering correction.

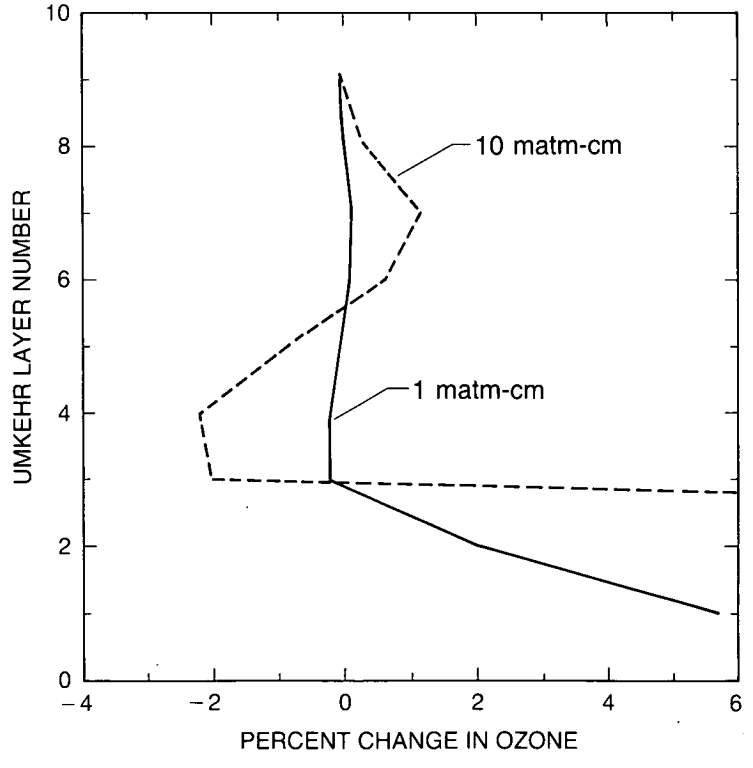

Figure 3.17. Sensitivity of the Umkehr-retrieved profile to SO_2 in the lower half of layer 1.

algorithm. If the necessary information is not available, then the problem is best handled by statistical methods; again, not a problem to be discussed in this chapter.

Nonlinearity errors have been discussed in Sections 3.3.4.3 and 3.3.4.4. Although such errors are not systematic in individual cases, they should average out to a roughly systematic error in trend estimation.

The "no refraction" assumption will lead to a systematic error such that derived ozone amounts in the uppermost layers are too low. This is understandable because the slant path attenuation is always decreased when refraction is added, and the scattering layer is always lower in the atmosphere for the longer wavelength of the pair, leading to a higher N-value at the larger zenith angles where the effect is greatest. The error is probably small, but it may depend, to some extent, on the amount of ozone at upper levels, thereby leading to an over- or underestimation of 40 km trends. This trend impact should be very small.

3.3.4.6 Trend Estimation Assessment

Many of the sources of error are unimportant for trend estimation because they should average out over the network, or over time, as instruments are periodically recalibrated, or if they have constant systematic errors. The important error sources are the sensitivities to atmospheric quantities that may have their own trends. It is unlikely that any instrumental parameter will have a trend that is repeated across the network. However, we should always be aware of sampling problems with a small network.

It is important to understand how true trends are reflected in the retrieved trend quantified by the averaging kernels, which indicate that the Umkehr retrievals for layers 4 through 8 (63–2 mb, 19–43 km) correspond to means over layers ~2.5 layers (12.5 km) thick, centered on approximately the correct nominal altitude. Outside this altitude range, and at higher vertical resolution, information about trends should be treated with caution. This is important, since the postulated chlorofluoromethane (CFM) effect will occur in layer 8 of the atmosphere. Retrievals from the standard Umkehr algorithm may show ozone being displaced upward in the atmosphere.

The most important quantities that may have trends unaccounted for in the Umkehr retrieval scheme are stratospheric aerosol, tropospheric pollution, and temperature.

Amounts of stratospheric aerosols, which vary with time, are undoubtedly the most important source of error in the long-term trend determination from Umkehr. Attempts have been made to do a first-order correction using the Mauna Loa Sun-sensor data. More recently, lidar measurement results are being used to obtain better corrections for the time period following the El Chichón eruption. However, the accuracy of the correction schemes used so far is still an open question.

Background urban tropospheric SO_2 levels (1 matm-cm) will cause negligible error in layers 4 to 8, but moderately heavy pollution (10 matm-cm) may cause errors of about 1 percent. As this is likely to be confined to a few heavily polluted urban areas, it is unlikely to be important for global trends, unless a significant number of stations are in polluted areas.

A false change of 1 percent in ozone in layers 4 to 8 would require a change of 10–15K in stratospheric temperature. This is unlikely to be a source of significant uncertainty.

3.3.5 Stratospheric Aerosol and Gas Experiment

The SAGE measures extinction of solar radiation in a limb path in the wavelength region from 380–1,020 nm. SAGE–II, currently in operation, measures sunrise and sunset extinction at seven wavelengths: 1,020, 936, 600, 525, 452, 448, and 385 nm. Those important for determining the altitude distribution of ozone are the aerosol-sensitive wavelengths of 1,020, 525, and 385 nm, and the ozone-sensitive wavelength of 600 nm. It is important to note that other measured constituents, such as NO_2, also contribute to the extinction at these wavelengths, if only slightly.

SAGE–II data have not yet been archived with NSSDC, but have been made available to the Ozone Trends Panel; it is the algorithm by which this data set was processed that is discussed here. SAGE–I was an instrument similar to SAGE–II, but with only four spectral channels, at 1,000, 600, 450, and 385 nm. The original inversion algorithm (Chu and McCormick, 1979), corresponding to the data in the NSSDC archive, is significantly different from that used in the SAGE–II data reduction. Because of the recent effort in ozone trend work, SAGE–I data have been reprocessed using an algorithm similar to the one used for SAGE–II; the reprocessed data are used in this report for comparison with other ozone data. The following discussions about the SAGE–I inversion algorithm will be understood to refer to the reprocessing algorithm.

The instrument has a field of view of 0.5 minutes of arc, which corresponds to 0.5 km at the limb. The instrument scans the solar disk during each measurement sequence to produce vertical profiles of constituent extinction. During a measurement sequence, the SAGE radiometer scans the Sun from top to bottom, as viewed from the spacecraft, at a scan rate of 15 minutes of arc per second. The Sun is scanned about 20 times for a normal sunset or sunrise event. Each channel is sampled 64 times per second and digitized to 12 bits.

Neither SAGE–I nor SAGE–II produces complete global data sets; thus, it is difficult to separate seasonal and long-term trends from the respective data sets. The first use of the SAGE data, therefore, is in a comparison with SBUV when both instruments observe the same ozone field. This comparison yields the long-term differences in calibration or changes in the relative bias between the two instruments.

3.3.5.1 Forward Model

The irradiance H_λ measured by the instrument at a given time t is given by

$$H_\lambda = \int_{\Delta\lambda}\int_{\Delta\Omega} I_{0\lambda} W_\lambda(\theta,\phi) F_\lambda(\theta,\phi,t) T_\lambda(\theta) d\Omega d\lambda \tag{26}$$

where $I_{0\lambda}$ is the incoming solar spectral radiance, W is the radiometer's FOV function, ϕ is the azimuthal angle, Ω is the solid angle, T is the transmittance of the atmosphere as a function of view angle θ, and F is the extraterrestrial solar radiance for wavelength λ. The mean transmittance over the spectral bandwidth and instrument field of view is obtained by dividing the irradiance measurements by those for a solar scan above the atmosphere. The transmittance function in terms of the minimum ray height is given by

$$T_\lambda(h) = \exp\left[-\int \beta_\lambda(h) dl_\lambda(h)\right] \tag{27}$$

where β is the total extinction coefficient of the atmosphere as a function of altitude h, and l is the geometric path length corrected for refraction.

The total extinction at each altitude is a linear combination of the extinctions of each constituent measured.

$$\beta_\lambda = \beta_R(\lambda) + \beta_{O_3}(\lambda) + \beta_{NO_2}(\lambda) + \beta_A(\lambda) \tag{28}$$

where $\beta_R(\lambda)$ is the extinction coefficient for Rayleigh scattering, $\beta_{O_3}(\lambda)$, $\beta_{NO_2}(\lambda)$, and $\beta_A(\lambda)$ are the extinction coefficients for ozone, nitrogen dioxide, and aerosol, respectively. It is assumed that there are no other constituents contributing to the extinction. For ozone and nitrogen dioxide, the extinction coefficient is given by the product of the number density and the absorption cross-section at the given wavelength.

The aerosol extinction coefficient is a function of aerosol size distribution, shape, and index of refraction. The following formula applies to homogeneous, spherical particles:

$$\beta_A(\lambda) = \int_0^\infty \sigma(n,r,\lambda)N(r)dr \tag{29}$$

where $N(r)$ is the size distribution function and $\sigma(n,r,\lambda)$ is the extinction cross-section for a particle with refractive index n and radius r, as computed from Mie theory. Because of the finite number of spectral channels being used, only a limited amount of information on either the aerosol size distribution or the wavelength-dependent extinction coefficient can be deduced. The refractive index is assumed to be 1.43, corresponding to sulfuric acid aerosol.

3.3.5.2 The Inverse Method

The procedure for inverting the SAGE–II data follows the approach taken in the inversion of the SAGE data, the basic algorithm for which is discussed by Chu and McCormick (1979). A two-step technique is used. The line-of-sight transmission measurements at the seven wavelengths are first separated into optical depths for each species, separately for each tangent altitude. These line-of-sight optical depths are then inverted for each species to give vertical profiles, assuming horizontal homogeneity.

After calibration, the data consist of optical depths at each wavelength, for each tangent height. Each is a linear combination of the line-of-sight absorber amounts of O_3, NO_2, the aerosol optical depth at each wavelength, and the Rayleigh-scattering optical depth. The tangent heights for the measurements are calculated from the satellite ephemeris and time in the case of SAGE–II. In the case of SAGE–I, this is not accurate enough; the height reference is obtained by matching the retrieved density profile with that calculated from the U.S. National Meteorological Center (NMC) data. The Rayleigh-scattering optical depth is calculated for each tangent ray using atmospheric temperature, pressure, and height data supplied by NMC, based on both radiosonde and satellite measurements. It is then removed from the measurements. The NO_2 component is calculated from the differential measurement supplied by the 448 nm and 453 nm data and removed from the measurements. The resulting five channels (ignoring the 954 nm water vapor channel, which is dealt with separately) are then used to solve for the ozone optical depth at 600 nm and for the four aerosol optical depths at 1020, 525, 453, and 385 nm.

The procedure for separating the ozone optical depth at 600 nm from the aerosol contribution is as follows: representing the aerosol size distribution $N(r)$ at a finite number of sizes $r_j, j = 1...m$, the aerosol extinction at the four wavelengths can be written as

$$\beta_i = \sum_{j=1}^{m} \sigma_{ij}(n)N_j \qquad i = 1...4 \tag{30}$$

which is an underconstrained set of linear equations for N_j. These can be solved using Twomey's minimum information solution (1963)

$$\mathbf{N} = \mathbf{K}^T(\mathbf{K}\mathbf{K}^T + \Gamma)^{-1}\beta \tag{31}$$

where $\mathbf{K}$ is a matrix with elements σ_{ij}, $\mathbf{N}$ is a vector with elements N_j, and Γ is a diagonal matrix with elements proportional to the estimated noise level at each aerosol wavelength. The aerosol extinction at 600 nm can then be expressed as a linear function of the retrieved $\mathbf{N}$, and hence as a combination of the extinction values at the other four wavelengths:

$$\begin{aligned} \beta_{600} &= \mathbf{K}_{600}\mathbf{N} \\ &= \mathbf{K}_{600}\mathbf{K}^T(\mathbf{K}\mathbf{K}^T + \Gamma)^{-1}\beta \\ &= \mathbf{a}\beta \end{aligned} \tag{32}$$

The four coefficients a_i can be precomputed, assuming only that the scattering is due to Mie particles with given refractive index. The aerosol extinction cross-section is calculated with the anomalous diffraction approximation.

The line-of-sight optical depth profile for each species is inverted using Twomey's modified Chahine algorithm (Twomey et al., 1977). The vertical profile for each species is represented by its averaged extinction in homogeneous slabs of 1 km thickness. Therefore, the line-of-sight optical depth for each species can be expressed as the product of a path-length matrix with each extinction profile. Since the measured signals for all channels decrease at a higher altitude, a 5 km vertical smoothing of the retrieved profile at high-altitude level is performed during each updating cycle in the inversion algorithm. Iteration is stopped when the residue between the measurement and the calculated optical depth approaches the estimated measurement uncertainty.

The primary difference between the SAGE–I and the SAGE–II inversion algorithms is the separation of optical depth values for aerosol, ozone, and NO_2. Because of the limited number of channels on SAGE–I, insufficient information is available to give a good description of aerosol optical depth versus wavelength behavior. In addition, the aerosol has almost the same spectral variation as NO_2 between 450 and 385 nm, thus making their separation impossible if only the measured data are used. In the SAGE–I algorithm, aerosol optical depth values at 450 and 385 nm are assumed to be a constant multiple of the values at 1,000 nm for altitudes above 27 km. The constants are determined assuming the aerosols are log normal distributed with refractive index $n = 1.43$, mean radius $r = 0.07\ \mu$m, and spread $\sigma = 1.8$ ($\log \sigma = 0.59$). Similarly, the NO_2 optical depth values below 27 km are calculated assuming constant NO_2 density. The aerosol optical depth values at 600 and 385 nm are then estimated with the same method as in the case of SAGE–II.

3.3.5.3 Forward Model Assessment

The aerosol representation is restricted to spherical Mie particles with a uniform index of refraction. Effects due to nonspherical shapes and nonuniform refractive index or composition are not included.

Ozone absorption cross-section measurements from Penney (1979) are used here. In the UV, these differ from those of Hearn (1961) by about 5 percent, which could lead to a bias in the ozone values. For NO_2, the unpublished data by Johnston and Graham (1977) are used. The accuracy of

ozone absorption cross-section at 600 nm is probably within 5 percent, while the accuracy at wavelengths other than 600 nm is probably not better than 10 percent. For NO_2, the accuracy of the absorption cross-section at all wavelengths is not better than 10 percent. However, this will produce only a constant systematic error and will have little effect on trend studies.

Measurements by Penney (1979) and by Vigroux (1953) indicate that the ozone Chappuis band centered at 600 nm showed no temperature dependence, while data from Vassey and Vassey (1948) showed some variation with temperature. It is likely that the temperature dependence of the ozone absorption cross-section at the SAGE–II spectral region is small and insignificant for ozone trend estimation. For the NO_2 absorption spectrum, Bass's et al. measurements (1976) for wavelengths below 400 nm indicated about a 10 percent change between room temperature and −40°C. However, there are no measurements of temperature effect at the wavelengths used by SAGE–II (448 and 453 nm). Due to the small effect of NO_2 on SAGE–II ozone determination, it is unlikely to affect ozone trend studies.

3.3.5.4 Inverse Method Assessment

NMC Temperature Field

The Rayleigh contributions at all seven channels are calculated from the NMC temperature and pressure data. The NMC temperature data are derived mainly from rawinsonde data at altitudes of 30 km and below and from satellite soundings above 30 km altitude. The accuracy of the NMC temperature data being used by the SAGE–II inversion algorithm is believed to be about 1 percent at or below 10 mb, degrading to 6–7 percent at 0.4 mb pressure level. However, due to the small contribution of Rayleigh extinction at 600 nm, the basic SAGE–II inverted product—ozone number density versus geometric height—is not sensitive to temperature error. Large error could be introduced if the results were converted to an ozone-mixing ratio at fixed pressure levels, as is needed for carrying out intercomparisons with instruments (such as SBUV) that measure ozone on a pressure scale.

Aerosol Representation

Because of the location of the spectral channels on SAGE–II, the aerosol extinction values at 600 nm will be most sensitive to size distributions that are multimodal in nature. This would affect the ozone retrieval up to about 20 to 25 km in altitude, depending on latitude and the amount of volcanic dust in the stratosphere.

In the case of SAGE–I, this problem is much worse because there are fewer channels. The only compensating factor is that the aerosol content of the atmosphere during SAGE–I lifetime (pre-El Chichón) was lower by a factor of 5 to 10 compared to SAGE–II measurements.

Horizontal Inhomogeneity

Since SAGE uses a solar occultation technique, measurements are performed at a solar zenith angle of 90°. Horizontal inhomogeneity on a scale of a few hundred kilometers becomes an important issue for constituents exhibiting strong photochemical reactions. This will be true for ozone above 50 km altitude during the sunrise and sunset measurement events. Other short-term, transient events that can lead to horizontal inhomogeneity in the ozone distributions could occur during sudden warming events. Similarly, cirrus clouds and Polar Stratospheric Clouds (PSC's) are likely to be horizontally inhomogeneous.

SAGE–I NO_2

The assumption of constant NO_2 density below 27 km restricts the available NO_2 information to 30 km or above. The effect on the aerosol data at 450 nm is not great because of the large differences in signal levels.

3.3.5.5 Error Analysis

The fundamental vertical resolution of SAGE is very high, as illustrated by the SAGE–II averaging kernels in Figure 3.18. These are very close to ideal—i.e., unity at the nominal altitude and zero elsewhere, from 20 km to 50 km. Below 20 km, the response to real changes in the atmosphere is somewhat reduced and broadened. Above 50 km, the noise on an individual profile is poor, so the vertical resolution has been deliberately reduced.

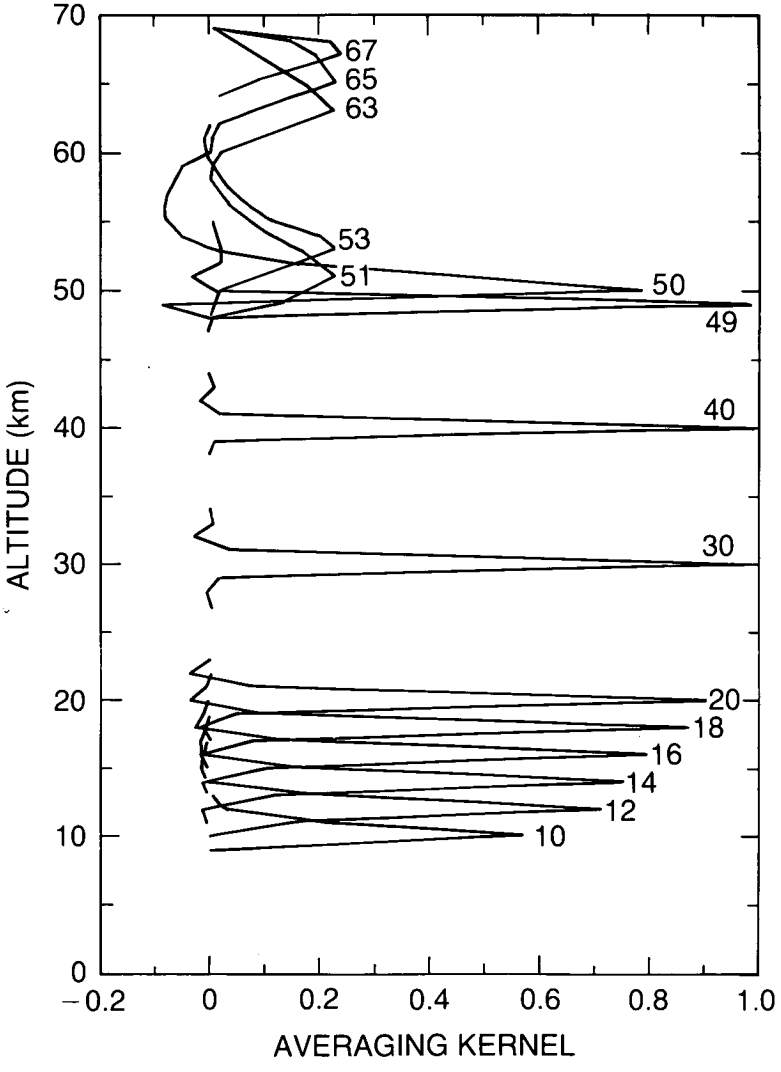

Figure 3.18. Averaging kernels for SAGE–II. Curves are not plotted for all altitudes.

For SAGE, the random error in the profile may be significant for trend estimation because it is a solar occultation measurement, and there are a maximum of two measurements per orbit. An estimate of this quantity, using only measurement error as sources of noise, is given in Figure 3.19. It is necessary to average more than 100 profiles for this source of error to become unimportant at the level of accuracy required for trend estimation.

The forward model parameters that may lead to profile errors include the extinction coefficients, the NMC temperature profile, and the registration of the profile in altitude. There is no opportunity for drift in radiometric calibration because a good zero and full-scale measurements are obtained at every occultation (see Chapter 2). Extinction coefficient errors may lead to trends in NO_2 or aerosol being aliased into trends in ozone. Temperature profile errors will lead to retrieval errors through both the Rayleigh correction and the temperature dependence of absorption coefficients.

Sensitivity of the retrieved profile to altitude registration is shown in Figure 3.20. Typical accuracy of the registration of SAGE–II is believed to be 100 m; it is not subject to long-term drift errors (unless there is unaccounted drift in the spacecraft clock and tracking), and thus will not contribute to trend estimation errors. The altitude registration accuracy for SAGE–I is believed to be about 150 to 200 m.

Sensitivity to the temperature profile is shown in Figure 3.21. One curve is shown for temperature at each of the standard levels from 300 mb to 0.4 mb. Above 20 km, the effect is very small and would not contribute to ozone trend errors, even for large trends in the error of the NMC temperature profile.

An error in the NO_2 differential absorption coefficient could lead to an incorrect NO_2 correction, and hence to an error in the O_3, which depends on the NO_2 amount. However, the NO_2 cross-section at 600 nm is only 5.5 percent of that at 448 nm, so this effect will be small.

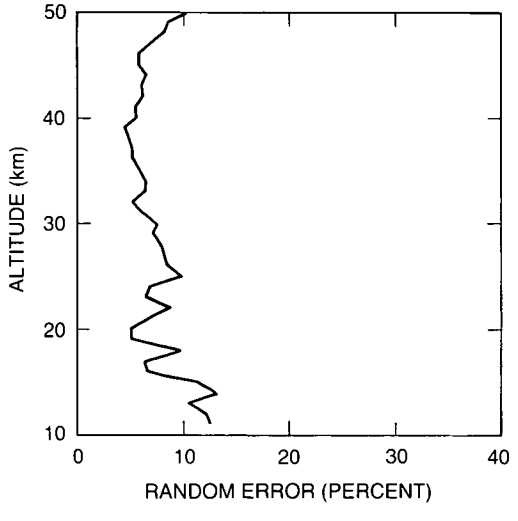

Figure 3.19. Random error of a single SAGE–II profile due to instrument noise only.

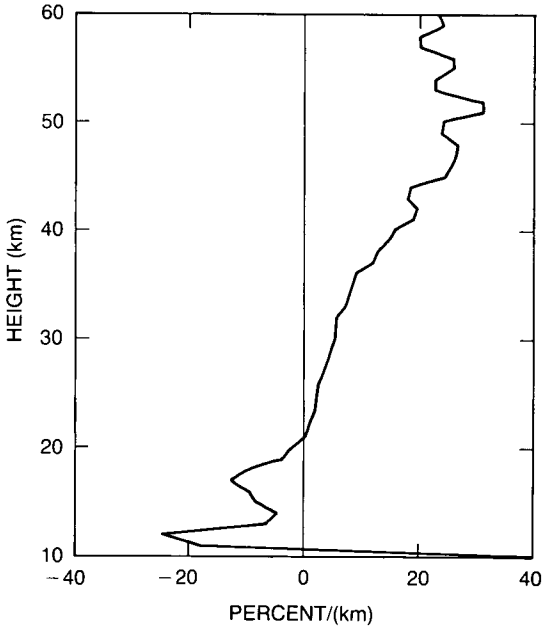

Figure 3.20. Sensitivity of the SAGE retrieval to altitude reference error.

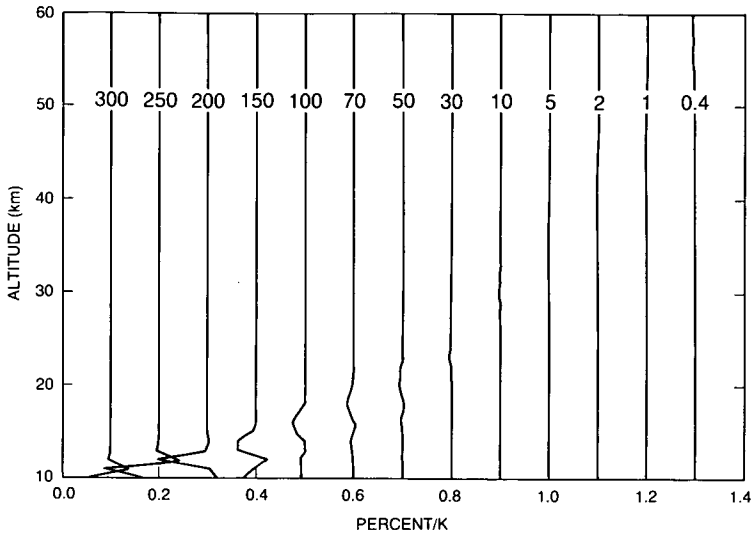

Figure 3.21. Sensitivity of the SAGE retrieval to atmospheric temperature errors. Curves are labeled with the pressure level (mb) at which the NMC temperature is perturbed and are offset by multiples of 0.1%/K for clarity.

3.3.5.6 Trend Estimation Assessment

SAGE–II data sampling is limited to 2 events per orbit, or 30 events per day. A latitudinal sweep in coverage for each event (sunrise or sunset) from about 80°S to 80°N takes about 3 weeks. The sampling frequency varies with latitude, with most sampling occurring at 80°N or 80°S, and less in between. With such a low and irregular sampling rate, SAGE data cannot easily be used for trend estimation, but can be used to assess the drift in other instruments, primarily the SBUV. Once a statistically meaningful sample is obtained, the SAGE–II data can be used for investigating trends.

The altitude range over which SAGE–II ozone data are relatively insensitive to other perturbations (i.e., aerosol correction at low altitude and photochemical correction at high altitude) is between 25 km and 50 km. Typical altitude resolution is about 1 km. The precision for each ozone profile in this altitude range is about 10 percent, while the systematic error (primarily the absorption cross-section uncertainty plus knowledge of the SAGE–II spectral filter response) could be up to 8 percent.

Other trends that can alias into the ozone include aerosol and temperature trends. Aerosol has been seen by the SAGE–II data processing team to alias into ozone in preliminary retrievals, when the aerosol correction for the ozone channel was not done correctly. This aliasing was evident in altitudes up to about 25 km at the low-latitude region from 1984 to 1985 because of remnant from El Chichón. The effect of a temperature trend is probably not significant when the SAGE–II ozone profile is restricted to altitudes below 50 km.

It is possible to estimate a trend from the difference between the SAGE–I and SAGE–II climatologies (for example, see Chapter 5). The accuracy of this trend will depend on the difference in systematic errors between the two instruments, the most important one probably being the treatment of the altitude reference. A preliminary analysis shows that SAGE–I heights may be around 90 m greater than those of SAGE–II, leading to a 2.5 percent error in the SAGE–I/SAGE–II ozone difference at 50 km.

3.3.6 Solar Mesosphere Explorer UV Spectrometer

A data set from the SME UV Spectrometer (SME–UVS) for 1982 to 1985 has been archived with NSSDC; however, it suffers from a drift in the sensitivity of the UVS, which leads to a drift in altitude registration, and hence a false trend in ozone. This section refers to a reprocessing, the results of which have been made available to the Ozone Trends Panel and will be placed in the archive in the near future.

3.3.6.1 Forward Model

As described in Rusch et al. (1984), hereinafter referred to as the Basic Reference (BR), and in Chapter 2 of this report, this experiment involved the measurement of the radiance of solar ultraviolet radiation scattered by Earth's limb in two channels (265 and 296.4 nm) with a half-width of approximately 1.5 nm. As the satellite spins, the radiances are measured for a series of lines of sight that have tangent heights, at the limb, ranging from 0 to 100 km. The response function for the measurement has a full width at half maximum of 3.5 km in the vertical. The radiance measurements are sensitive to ozone density changes within the altitude range from about 48 to 68 km, varying somewhat with solar zenith angle.

The limb-viewing geometry is illustrated in Figure 2.33 in Chapter 2. The forward model (see Equations (1), (2a), (2b), (2c) in BR) involves a numerical quadrature calculation of primary Rayleigh scattering in a thin-shell, horizontally homogeneous, spherical atmosphere containing absorbing ozone and scattering air molecules, but no aerosols. This is similar to SBUV and Umkehr, but with a different geometry.

The ozone absorption cross-sections of Bass and Paur (1985) are convolved with the instrument slit functions to obtain effective absorption cross-sections for each channel. The temperature effect is very small at 265 nm (.03%/°C) and small at 296.4 nm (0.1%/°C). The molecular-scattering cross-sections of Penndorf (1957) and Bates (1984) were convolved with the instrument slit functions to obtain effective cross-sections for each channel. The effects of aerosol scattering and absorption by molecules other than ozone, resonance fluorescence, and scattering by other atmospheric gases are omitted (see Section 3.3.3 on SBUV for a discussion of this effect).

The solar flux values measured in a separate experiment on SME (Rottman et al., 1982) were used in the calculation of radiances. Absolute error of these fluxes is estimated to be ± 10 percent, with relative error of ± 1 percent.

The MAP model atmosphere (Barnett and Corney, 1985) was used for the air density profile. This model specifies monthly averages of temperature, pressure, and density as a function of altitude; the algorithm uses a cubic spline fit to obtain data for any specific day, assuming the monthly averages apply to the middle of the month.

As with any limb experiment, a critical phase of the data evaluation is the assignment of an altitude or pressure to each measurement point in a scan. The following (updated) quotation from BR (p. 11684) describes the procedure used in the UVS experiment.

The absolute direction of the line of sight of the scientific instruments is determined from an analysis of averaged pitch angles derived from the four horizon sensor crossings each spin. This analysis leads to limb altitude determinations with residuals of the order of 1 km at a slant distance of 2,550 km (Cowley and

Lawrence, 1983). The limb altitudes are further refined by comparisons of the Rayleigh-scattered radiance measured by the UVS with that calculated from modeling this signal using the relevant solar fluxes, cross-sections, and the MAP model atmosphere. The normalization in altitude is done at 65 km in the long wavelength channel (296.4 nm), where no ozone absorption is detectable and the Rayleigh-scattering signal is optically thin.

Rusch advises that, in fact, one or two radiances above 65 km may be included in the normalization procedure for improved accuracy. In a sense, this procedure could be considered a direct measurement of the pressure at the tangent point.

The radiance quadrature is carried out over the field of view of the instrument by assuming horizontal homogeneity and integrating in the vertical at 3.5 km intervals, using a four-point Lagrangian interpolation. The variation of the instrument sensitivity over the FOV is included in the quadrature. In addition, the polarization sensitivity of the long-wavelength channel is applied in the radiance calculation for that channel. The short wavelength channel has no measured polarization sensitivity (Figure 6 of BR). With the tilting of the FOV, the quadrature becomes slightly more complex because the sum for each 3.5 km interval has a different weight, depending on the amount of the tilt.

In preparing observed data for inversion, a minimum of five and a maximum of six radiance profiles are averaged to ensure "adequate counting statistics." This is consistent with a latitude resolution of about 5°. In addition, there is an inherent "smearing" along the line of sight in the limb technique.

3.3.6.2 The Inverse Method

The equations to be inverted are linearized in terms of a departure from a first-guess ozone profile (Krueger and Minzner, 1976), computing radiances, and first-order partial derivatives of radiance with respect to layer ozone density. Since the radiative transfer equation is nonlinear, the problem is solved iteratively. The solution involves Twomey's (1963) minimum departure from the first-guess profile.

We define the matrix of first order partial derivatives, $\mathbf{K}$, by

$$K_{ij}^{n} = \frac{\partial y_i^n}{\partial x_j^n} \tag{33}$$

where n refers to the iteration number, y_i^n is the calculated radiance at a wavelength and tangent height indexed by i, and x_j^n is the ozone density at layer number j.

The solution is given by

$$\mathbf{x}^n = \mathbf{x}^{n-1} + (\mathbf{K}^T\mathbf{K} + \Gamma)^{-1}\mathbf{K}^T(\mathbf{y}_{obs} - \mathbf{y}_{cal}^{n-1}) + \Gamma(\mathbf{x}^0 - \mathbf{x}^{n-1}) \tag{34}$$

where $\mathbf{K}$ is calculated at $\mathbf{x}^{n-1}$, $\mathbf{y}_{obs}$ is the measured radiance vector, $\mathbf{y}_{cal}^{n-1}$ is the radiance calculated using $\mathbf{x}^{n-1}$, and Γ is a diagonal matrix with Twomey's smoothing vector on the diagonal. The iterative procedure is terminated when the elements of the residual vector $(\mathbf{y}_{obs} - \mathbf{y}_{cal}^{n-1})$ are reduced below the measurement noise level. This convergence criterion is not strictly correct, but it will lead only to random errors and occasional failures to converge, and does not matter for trends studies.

The SME–UVS radiance measurements are sensitive to ozone density changes within the approximate altitude range of 46 to 68 km. For tangent heights above about 68 km, there is insufficient ozone to affect the measurement at 265 nm. For tangent heights below about 46 km, 296.4 nm photons received at the satellite have been scattered mostly from altitudes above the tangent height; the radiances, therefore, contain no information about ozone at the tangent height. The elements of the smoothing vector are set to zero in the central part of the good information region and are increased sufficiently beyond the boundaries to ensure that the first-guess profile is returned outside the good information range and to avoid instabilities in the solution.

The algorithm solves for the mean ozone densities in 2 km layers centered at heights of 48, 50, . . . 68 km. The lower altitude information limit for the 265 nm channel and the upper altitude information limit for the 296.4 nm channel roughly coincide at about 58 km.

A second algorithm was developed to reduce the data taken after the beginning of 1987 because fewer independent pieces of information were available in the measurements, as a result of the poorer resolution with the spin axis tilting (we note that a similar end result could have been achieved by an increase in the elements of the smoothing vector). In the new algorithm, both the first-guess $x^0(z)$ and the iterated solution $x^n(z)$ are specified as the exponential of a polynomial

$$x^n(z) = \exp[a_1^n + a_2^n(z - z_0) + a_3^n(z - z_0)^2 + a_4^n(z - z_0)^3] \tag{35}$$

where z is altitude, $z_0 = 48$ km is a reference altitude, and a_i^n $(n>0)$ are the unknown polynomial coefficients to be determined at iteration n. As a first guess, a_3^0 and a_4^0 are taken to be zero. For calculating the radiances and the partial derivatives, the profile is taken to be a linear combination of the first guess and the solution profile on the last iteration.

$$x^{*n}(z) = B(z)x^n(z) + [1 - B(z)]x^0(z) \tag{36}$$

where $B(z)=1$ for $48<z<69$ and tends to zero smoothly outside this range. The procedure is exactly as before but with all elements of the smoothing vector set to zero

$$K_{ij}^n = \frac{\partial y_i^n}{\partial a_j^n} \sum_k \frac{\partial y_i^n}{\partial x_k^n} \frac{\partial x_k^n}{\partial a_j^n} \tag{37}$$

$$\mathbf{a}^n = \mathbf{a}^{n-1} + [\mathbf{K}^T\mathbf{K}]^{-1}\mathbf{K}^T(\mathbf{y}_{obs} + \mathbf{y}_{cal}^{n-1}) \tag{38}$$

and the iteration procedure is stopped using the same criterion as before. This is an ordinary least-squares solution.

3.3.6.3 Forward Model Assessment

Single Scattering Approximation

The worst case error in calculated radiances is probably less than 1 percent due to neglect of multiple scattering. The quadrature error in this calculation does not appear to have been directly assessed in the BR.

Neglect of Refraction

This is negligible at these altitudes.

Ozone Cross-Sections

Experimenters estimate the uncertainty at 5 percent, although, at these wavelengths, the error is likely to be less than 3 percent. Bass and Paur (1985) estimate their measurement error to be less than 1 percent. However, their measurements are relative to that of Hearn (1961) at 253.7 nm, which is believed to be within 2–3 percent (Hudson, private communication).

Rayleigh Scattering Cross-Sections

Bates (1984) estimates that his values are within 1 percent.

Omission of Aerosols

Polar mesospheric clouds produce obvious anomalous effects; these cases are discarded in the data evaluation. The possible effects of background mesospheric aerosols at heights at and above 48 km are difficult to assess. There are no measurements of particle size distribution at these levels, and the presence of aerosols is very difficult to detect. If such background aerosols do exist, they are likely to be variable; derived ozone densities may be too low and exhibit spurious variability. Aerosols have been detected at altitudes below 48 km (Clancy, 1986). Such aerosols could affect results by increasing the small multiple-scattering error.

Other Scattering Mechanisms

Resonant and Raman scattering and scattering by other atmospheric gases have not been included in the forward model; see Section 3.3.3.3 for a discussion of this effect.

3.3.6.4 Inverse Method Assessment

This assessment refers primarily to the original algorithm.

The first-guess profile is the Krueger–Minzner (1976) midlatitude Northern Hemisphere profile. The choice of first guess should not affect the retrieved profile within the validity range of altitude of the experiment. However, this is not specifically stated by the experimenters.

The customary $\mathbf{S}_x$ and $\mathbf{S}_\epsilon$ covariance matrices are not used explicitly in the inversion procedure, although their implied general characteristics may be inferred from the smoothing vector elements. The smoothing vector is designed empirically to retrieve the first-guess profile outside the information range and the true profile (within error bounds) within the information range, and to have a smooth transition in between.

3.3.6.5 Error Analysis

The SME–UVS team has not been able to provide the standard diagnostics at the time of writing this chapter; therefore, we summarise here the analysis of random and systematic errors in the retrieved profiles from the BR. We have not confirmed this analysis.

Random errors include photon counting errors (noise), data compression before transmission to ground, real atmosphere differences from the model atmosphere, and errors arising from altitude–radiance normalization. In the analysis, the first two and last two of these are considered together. The first two combined produce errors in the retrieved profiles ranging from about 3 percent at 48 km to about 10 percent at 68 km, while the second two combined produce 4 and 10 percent at the lower and upper levels, respectively. When all four are combined, the total random error ranges from about 6 percent at 48 km to about 14 percent at 68 km (See BR Table 2 and Figure 10a).

The systematic errors include absolute instrument calibration (but solar flux error has not been included here), measurement of instrument polarization, measurement of PMT dead time, and ozone cross-section. The first of these, assumed to be 10 percent for instrument calibration, produces the dominating systematic error component of about 17 percent from 50 to 62 km, decreasing somewhat above and below this range. Since solar flux instrument calibration error was not included, this result really applies to the (radiance–irradiance) ratio. This error results from the dependence of the reference density level, nominally at 65 km, on the instrument gain. If the true gain is larger than that given by the calibration (positive error), the scattered UV radiance calculated for the reference level in the model atmosphere will be sensed from a lower density level (higher altitude). Because ozone density decreases more rapidly with height than atmospheric density, the ozone error is larger than the calibration error, as well as being of opposite sign. When the remaining error components are included, assuming no correlation between the different error types, the total systematic error is just over 18 percent from 50 to 62 km (see BR, Table 3, Figure 10b, and Chapter 2).

3.3.6.6 Implications for Trend Estimation

Trend estimation will be compromised by the total relative in-flight drift of UVS and Solar Flux instrument calibrations (PMT sensitivity and dead-time constant). In each case, this includes any relative drift of calibration between the two wavelength channels. A +1 percent per year drift in the (radiance–irradiance) ratio will produce a fictitious ozone trend of −1.7 percent per year.

Real trends in atmospheric temperature within the 48–68 km altitude range will produce only small effects in this range through the absorption cross-section temperature dependence in the 296.4 nm channel (+1°C per year produces +0.1 percent per year fictitious ozone trend). A more important contribution may arise through temperature changes at any altitude below 68 km, as this affects the pressure–height relationship through the hydrostatic equation. It would then be possible for derived ozone densities to be assigned to the wrong altitude. A symptom of this effect could be a drift in the radiance–height matchup at 65 km. This symptom, however, would apply also to a net relative calibration drift as described above. Monitoring this matchup could be a good first-order diagnostic of possible problems.

A change in background mesospheric aerosol may introduce a fictitious ozone trend of a sign that depends on optical properties. We assume that obvious cases of polar mesospheric clouds are correctly detected, then rejected from processing.

3.3.7 Solar Mesospheric Explorer Near Infrared Spectrometer

The Solar Mesospheric Explorer Near Infrared Spectrometer (SME–NIRS) measures infrared limb emission by excited oxygen ($O_2(^1\Delta_g)$) at 1.27 μm—the result of photodissociation of ozone

by ultraviolet radiation and subsequent photochemical reactions. The analysis of the data is complicated by the fact that some of the $O_2(^1\Delta_g)$ molecules are quenched by collisions with the major atmospheric molecules, and that the other product of the photodissociation of ozone, $O(^1D)$, can produce $O_2(^1\Delta_g)$ indirectly by collision with molecular oxygen.

The SME–NIRS data set for 1982–1985 has been archived with the NSSDC. However, this data set suffers from a drift in the sensitivity of the SME–UV spectrometer, which leads to a drift in altitude registration, and hence a false trend in ozone. The data are being reprocessed with better values for the altitude registration and will be placed in the archive in the near future. The description below applies to both data sets.

3.3.7.1 Forward Model

The complete forward model has been described by Thomas et al. (1984) and will not be reproduced here in detail. It is assumed that the only reactions that occur are

$$\begin{aligned}
O_3 + h\nu(210<\lambda<310\text{nm}) &\rightarrow O_2(^1\Delta_g) + O(^1D) && \epsilon J_3 \\
O_2(^1\Delta_g) + O_2 &\rightarrow 2O_2 && k_D \\
O(^1D) + O_2 &\rightarrow O(^3P) + O_2(^1\Sigma) && k_O \\
O(^1D) + N_2 &\rightarrow O(^3P) + N_2 && k_N \\
O_2 + h\nu(\lambda = 762\text{nm}) &\rightarrow O_2(^1\Sigma) && J_s \\
O_2(^1\Sigma) + M &\rightarrow O_2(^1\Delta_g) + M && k_s
\end{aligned} \tag{39}$$

It should be noted that the J's are altitude dependent due to absorption of incoming solar radiation, and that the k's may be temperature and, therefore, altitude dependent. By solving the kinetic equations associated with these reactions, it can be shown that the volume emission rate V at an altitude h is given by

$$V(h) = \left\{ \frac{P_s k_s[M]}{A_s + k_s[M]} + \epsilon J_3[O_3] \right\} \frac{A_D}{A_D + k_D[O_2]} \tag{40}$$

where A_s and A_D are the spontaneous emission coefficients for the $O_2(^1\Sigma)$ and $O_2(^1\Delta_g)$ levels, respectively, and the $O_2(^1\Sigma)$ production rate P_s is given by

$$P_s = J_s[O_2] + \epsilon J_3[O_3] \frac{k_O[O_2]}{k_O[O_2] + k_N[N_2]} \tag{41}$$

Thus, the volume emission rate is a linear function of $J_3[O_3]$. The observed slant intensity for tangent height h_0 is related to the volume emission rate by an integral along the line of sight

$$S(h_0) = \int_{FOV} W(\theta - \theta_0) \int_0^\infty V(l,\theta) T(l,\theta) dl d\theta \tag{42}$$

where θ is scan angle, $W(\theta)$ is the FOV profile, and $T(l)$ is the transmittance along the line of sight from the emission at position l to the instrument, accounting for absorption by the O_2 ground-state molecules.

3.3.7.2 The Inverse Method

In preparing observed data for inversion, the good profiles are averaged together in sets of six. This merging reduces the latitude resolution to about 5°.

The instrument's line of sight is determined by relating the Rayleigh-scattered radiance near 70 km, measured by the SME–UV spectrometer, to that calculated from a model atmosphere, thus relating the altitude scale to a pressure reference. In the long term, the ultraviolet spectrometer sensitivity is tied to that of the visible spectrometer (see Chapter 2). Any degradation of the visible spectrometer will therefore be manifested as an altitude error. The inverse method is carried out in two parts. First, the observed line-of-sight radiances are inverted to yield volume emission rates as a function of altitude. Second, the volume emission rates are reduced to ozone profiles using the MAP model atmospheric temperature and pressure distribution (Barnett and Corney, 1985) and the assumed photochemistry.

The present inversion scheme uses a constrained linear matrix equation to solve for the volume emission rates. The constraint weighting for each layer is obtained from an empirical relation chosen to give a stable solution with the least possible constraint. It should be noted that the present scheme differs from the onion-peel approach described by Thomas et al. (1984).

The volume emission rate $V(h)$ is represented by a four-point Lagrangian interpolation between values at a set of levels spaced at 3.5 km intervals, expressed as a vector $\mathbf{v}$. The integral in Equation 42 for the line of sight radiance becomes a matrix product of the form $\mathbf{I} = \mathbf{F}\mathbf{v}$, where $\mathbf{F}$ depends on W and T. This equation is solved for $\mathbf{v}$ by least squares with the smoothing constraint that the vertical derivative of $V(h)$ is close to an average volume emission rate vertical derivative, $\overline{\Delta \mathbf{v}}$, by minimising

$$|\mathbf{I} - \mathbf{F}\mathbf{v}|^2 + w^2 |\overline{\Delta \mathbf{v}} - \mathbf{D}\mathbf{v}|^2 \tag{43}$$

where $\mathbf{D}$ is a matrix operator expressing vertical differentiation. The empirically determined weight w determines the relative importance of the smoothness constraint, increasing with α, the absolute value of the slit tilt angle

$$w(\alpha) = \frac{c|\mathbf{I}|}{2\overline{\Delta \mathbf{v}}\sqrt{n}} (1 + \tanh(b(\alpha/a - a/\alpha))) \tag{44}$$

The constants a, b, and c were chosen to give a stable solution with minimum constraint. Note that no constraint is placed on the value of the volume emission rate itself, only on its derivative.

The ozone profile is then derived from the volume emission rate according to Equations 40 and 41, using the assumed photochemistry and the climatological atmospheric temperature profile. This is not linear in O_3, as J_3 depends on the ozone above h, but it is straightforward.

3.3.7.3 Forward Model Assessment

The relationship between the measured quantity and the ozone profile is complicated; it depends on a complete understanding of the photochemistry involved. It is always possible that some significant constituent or reaction has not been considered, although we are not aware of any. The rate constants used in the SME analysis appear sound, but there are some concerns that can be raised.

$O_2(^1\Delta_g)$ Formation in the O_3 Photolysis

Not all of the photodissociation of O_3 leads to the production of $O_2(^1\Delta_g)$. The ratio used by SME is 0.9, based on the work of Fairchild et al. (1978). This ratio was not measured by observing

the $O_2(^1\Delta_g)$ emission, but by measuring the production of the $O(^1D)$ atom. There is some evidence that this may not give the same answer (Valentini et al., 1987). However, no explanation of the discrepancy has yet been given.

O_3 Photolysis Rate

The rate of 8×10^{-3} mols/sec given in Thomas et al. (1984) is a misprint. It should read 9×10^{-3} mols/sec, in agreement with other derivations.

Quenching of $O(^1D)$

The rates given in Thomas et al. (1984) for the quenching of $O(^1D)$ by N_2 and O_2 have the wrong temperature dependence, according to the original reference (Streit et al., 1976). The forward model also does not include the fact that not all quenching of $O(^1D)$ by O_2 leads to the production of $O_2(^1\Sigma)$; some of the reactions lead to a ground-state molecule. Harris and Adams (1983) give a branching ratio for the production of $O_2(^1\Sigma)$ of 0.77 ± 0.2. This branching ratio was obtained at room temperature, but it could be temperature dependent, and therefore different at mesospheric temperatures.

To test the sensitivity to temperature dependence, the correct temperature dependence has been put in the inversion; a 6 percent decrease in ozone resulted in most of the region. Adjusting the rates and adding the branching ratio was not done but would cause a small ($\sim$ 3 percent) increase in ozone.

Quenching of $O_2(^1\Delta_g)$ by O_2

The value chosen for the forward model for the quenching rate of $O_2(^1\Delta_g)$ by O_2 is that of Findlay and Snelling (1971). Wayne (1985) recently reviewed the measurements for this reaction. His preferred room temperature value for the rate is 1.56×10^{-18} compared with 2.22×10^{-18} used by SME. The temperature dependence of the reaction has been measured by Findlay and Snelling over a limited temperature range (285–322K), all above mesospheric temperatures. Thus, the values used by SME are from an extrapolation outside the measurement range. A decrease in quenching results in a corresponding decrease in the ozone by the same amount; this change would give a significant decrease (30 percent) in ozone.

Quenching of $O_2(^1\Sigma)$

The error bars assigned by SME to the quenching rate of the $O_2(^1\Sigma)$ by N_2 seem too large. Wayne (1985) recommends a value of 2.2×10^{-15}, which is close to the value of 2.0×10^{-15} used by SME.

3.3.7.4 Inverse Method Assessment

We have found no significant problems with the inverse method that might lead to errors in trend analyses based on SME–NIRS data. The only minor point is the use of a rather ad hoc constraint, which might be too loose or too tight. The averaging kernels in Figure 3.22a indicate that the constraint is probably too loose for single-profile retrievals at $\theta = 0$.

3.3.7.5 Error Analysis

The averaging kernels for the ozone mixing ratio on a pressure scale are shown in Figure 3.22a–c for three values of the slit tilt, θ, and for a set of levels spaced at intervals of 0.5 in $\log_{10} p$. The resolution is comparable with the FOV width (3.5 km) for $\theta = 0$, about 5 km at $\theta = 10°$, and about 10 km at $\theta = 25°$. We note that the resolution varies only slightly with altitude. There are significant negative excursions in all cases, although for $\theta = 0°$ they lie close to the main peak and may not be significant for trend estimation. For higher altitudes at $\theta = 25°$ (above about 0.005 mb), the negative excursions are serious; these data should not be used for trend studies.

Sensitivities to the forward model parameters are shown in Figures 3.23 and 3.24. The primary sources of random error are detector noise, digitization errors, and variations of the atmospheric temperature. Systematic errors include errors in the rates, cross-sections, the chemical reaction scheme, errors in the temperature climatology, and instrument calibration errors. Of these, the quantities that may be subject to trend errors are atmospheric temperature, altitude reference, and calibration (gain). The solar input $\epsilon J_{3\infty}$ will vary slightly with solar cycle, but with insignificant effect.

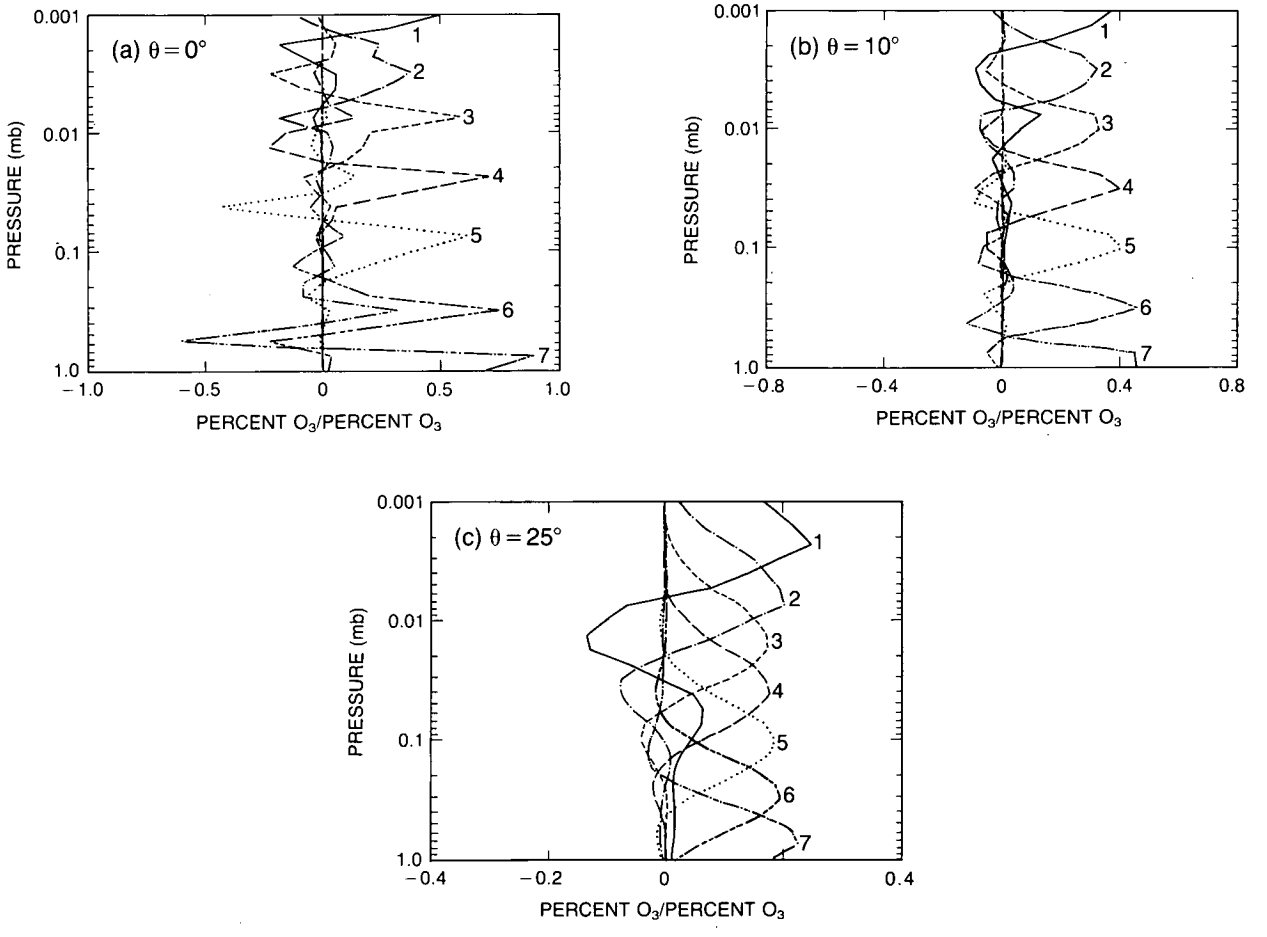

Figure 3.22. Averaging kernels for SME–NIRS at selected altitudes. (a) Slit tilt = 0°. (b) Slit tilt = 10°. (c) Slit tilt = 25°. The curves are labeled (1) 0.001 mb, (2) 0.0032 mb, (3) 0.01 mb, (4) 0.032 mb, (5) 0.1 mb, (6) 0.316 mb, and (7) 1 mb.

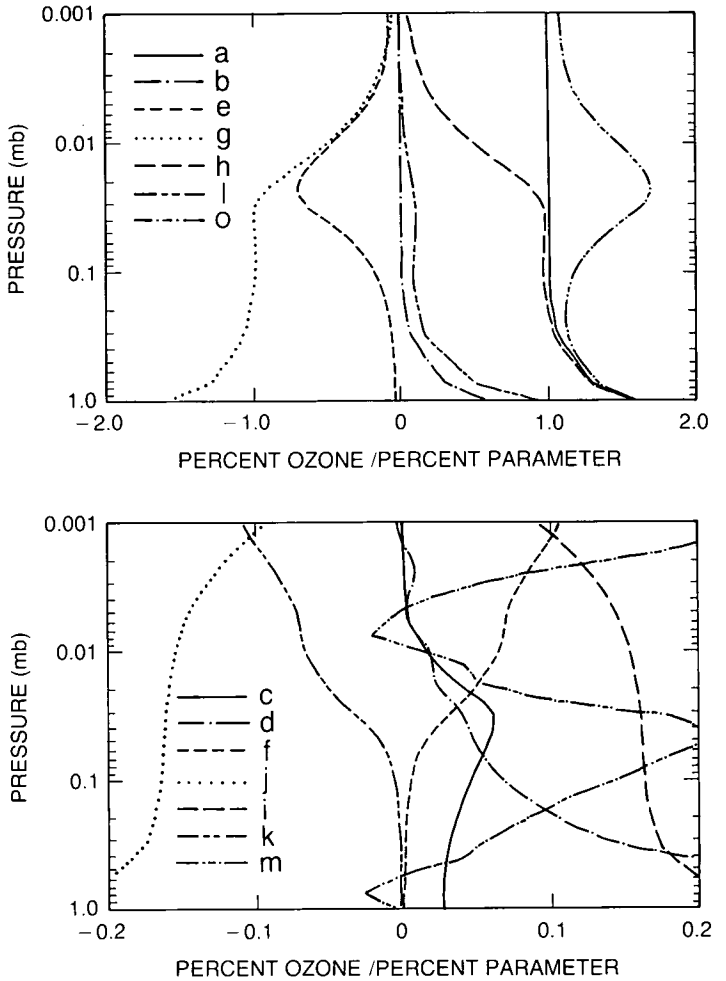

Figure 3.23. SME–NIRS sensitivities to model parameters at slit tilt = 0°. Units are percent ozone per percent parameter, except where stated. (a) $J_{3,\infty}$ (b) τ_{UV} (c) τ_{762} (d) $\tau_{1.27}$ (e) $J_{S,\infty}$ (f) A_S (g) A_D (h) k_D (i) k_N (j) k_O (k) k_S (l) Cal (m) Altitude reference (percent ozone per 0.01 km) (o) Solar zenith angle (percent ozone per 0.01 radian).

3.3.7.6 Trend Estimation Assessment

The SME–NIRS method is somewhat indirect, relying on a complete understanding of the relevant ozone photochemistry, including its temperature dependence. We have found no significant errors in the photochemistry, but it is always possible that some reactions have been omitted or misunderstood.

The SME–NIRS should be capable of measuring trends from around 50 km to around 90 km with a vertical resolution of about 4 km at the start of the mission, and then 10 km at the end, as a result of slit tilt. The averaging kernels at zero slit tilt are rather oscillatory and could be improved.

Drift in the retrieval caused by drift (around ± 0.18 km/year) in the reference altitude will be small at 1 mb, rising to about 4 percent per year at 0.05 mb. This is the largest source of uncertainty.

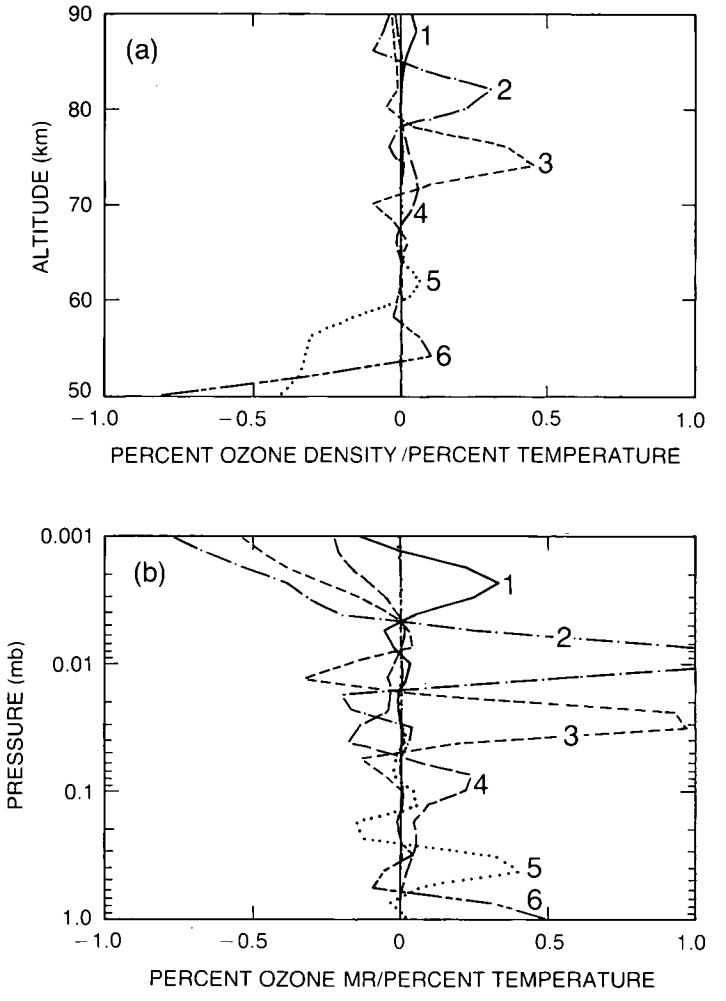

Figure 3.24. Sensitivity of SME–NIRS retrievals to temperature errors. (a) Density on a height scale (b) Mixing ratio on a log pressure scale. Plotted are the perturbations in the profile due to a 1K temperature change at (1) 90 km, (2) 82 km, (3) 74 km, (4) 66 km, (5) 58 km, and (6) 50 km.

Changing instrument calibration (<1%/yr) may lead to drifts of a similar magnitude in ozone.

Drift caused by real temperature changes, relative to the climatology used, would have to be 3–5K/yr to explain the +1.6%/yr change seen by the SME–NIRS measurements. Real temperature changes are likely to be rather less than this.

3.3.8 The Limb Infrared Monitor of the Stratosphere

The Limb Infrared Monitor of the Stratosphere (LIMS) experiment was launched on the Nimbus–7 spacecraft in October 1978, and produced data until May 1979. It measured concentrations of ozone and other gases in the stratosphere by measuring the limb-emitted radiation in selected spectral regions in the infrared (Gille and Russell, 1984). The spectral region covered by the LIMS radiometer ranged from 6 to 16 μm wavelength. Ozone measurements were obtained from the spectral channel centered at 9.6 μm. Two CO_2 channels, one wideband and one narrowband, centered at the 15 μm, were used to generate stratospheric temperature

profiles. The temperature profiles were then used in the reduction of data from all the other channels for the calculation of the Planck function term.

The LIMS radiometer scanned vertically at a rate of 0.25° per second. The data were sampled at a rate of one per 24 msec and digitized with a 12-bit A-to-D converter. The vertical instrument FOV for the ozone channel was 1.8 km when projected to the atmosphere at the tangent point location.

This discussion applies to the LIMS Version 5 algorithm, the results of which have been archived with NSSDC.

3.3.8.1 Forward Model

The limb radiance $I(h)$ measured by the LIMS instrument at a fixed tangent height h is given by (Gille and Russell, 1984)

$$I(h) = \int_{h-\Delta z}^{h+\Delta z} dz \int_{\upsilon_1}^{\upsilon_2} d\upsilon \int_{-\infty}^{\infty} dl B(\upsilon,\Theta(l))\phi(\upsilon)W(h-z)\frac{dT(\upsilon,l,h)}{dl} \qquad (45)$$

where $B(\upsilon,\Theta)$ is the Planck function at wavenumber υ and temperature Θ, l is distance along the line of sight, T is the infrared transmittance between l and the spacecraft, $\phi(\upsilon)$ is the instrument spectral response function, and $W(h-z)$ is the instrument field of view (IFOV) function.

The forward model for LIMS data retrieval is a numerical integration of Equation 45. Radiances are computed appropriate to the LIMS measurement geometry, at 1.5 km intervals (the same altitude interval as the homogeneous shell thickness used in the inversion). The Planck function is calculated from the temperature profile retrieved from the LIMS's two CO_2 channels (Gille et al., 1984a). The atmosphere is assumed to be in local thermodynamic equilibrium.

Limb path transmittance values are calculated with the emissivity growth approximation (EGA) scheme (Gordley and Russell, 1981). The most up-to-date line parameters for the ozone 9.6 μm band were used in the calculation of transmittance tabulation. The isotope line parameters of Drayson et al. (1984) were also included. No interfering species were included. The calculated $I(h)$ was smoothed with a Gaussian filter of width 1.1 km, to match the preconditioning applied to the measured radiances.

3.3.8.2 The Inverse Method

Preconditioning of the Radiances

The radiances subject to inversion were obtained from the radiometer measurements through a series of steps, the most important of which are discussed below.

The radiometer measurements were calibrated using the preflight data on the linearity of the radiometer and the black body source as described in Chapter 2. A correction for spacecraft rotation during the scan is inferred from a pair of up and down scans. The correction results in an effective change of the scan rate. Data are discarded if the required correction is larger than 4 percent of the nominal scan rate.

The radiance scan, with samples nominally every 0.375 km, were Fourier transformed and multiplied by the inverse transform of the IFOV and electronic filter. Thus, a correction for the effect of the IFOV sidelobes and the amplitude and phase rates of the electronic filter was applied in the frequency domain. In addition, the measurements in the different channels were co-aligned by this process; high frequencies were removed with a Gaussian apodization filter. These steps are described in Gille and Russell (1984) and Bailey and Gille (1986), although the details of the apodization in this paper differ slightly from that applied to the archived data.

The final filtered radiances were sampled at 1.5 km intervals for input into the inversion procedure.

The Inversion Procedure

The inversion procedure is basically an onion-peeling approach in which the solution profile is sought from the top to lower layers. In each layer, the solution is updated in an iterative manner, as described by Russell and Drayson (1972) and Bailey and Gille (1986). The radiances are compared to the calculated forward radiances at each layer. The first-guess solution for the top level is from the solution obtained from the previous scan, while for the lower levels, the first-guess solution is always from the previous higher level. During the iteration cycle, the solution at a particular level is updated with a partial derivative computed from the previous iteration. The convergence criterion for each level is that the relative difference between the filtered and the synthetic radiances is less than 0.1 percent.

The inversion procedure does not explicitly use a priori information, except for the smoothing implied by the preconditioning described above and a zero vertical derivative in ozone above the topmost level.

3.3.8.3 Forward Model Assessment

Ozone Line Parameters

The ozone 9.6 μm band strength is known to better than 8 percent. However, there are a large number of weak lines within the band with less accurate line parameters. Because of the limb geometry, the uncertainty of the calculated transmittance values due to line parameter errors is about 8 to 10 percent for altitudes above the ozone peak, increasing to 15 to 20 percent for altitudes below the ozone peak, due to the significant contributions from the less well-known weak lines (Drayson et al. 1984). However, emission errors can be larger when this effect is coupled with a steep positive lapse rate and optically thick paths, as in the equatorial lower stratosphere.

Transmittance

The accuracy of the emissivity growth approximation for calculating the limb transmittance is generally within a few percent, and the errors are smaller for weak and strong absorption.

Temperature

The error in the temperature values used is less than 2K, based on the retrieval of the two 15 μm CO_2 channels (Gille et al. 1984a). The inclusion of horizontal temperature gradient correction in calculating the limb transmittance is important.

Horizontal Gradients

Roewe et al. (1982) showed that horizontal gradients along the line of sight could have a large effect on the outgoing radiance at altitudes for which the optical depth from space to the tangent point along the limb viewing path is of order 1 or more. This paper further showed that gradients in trace constituents concentrations had a considerably smaller effect than temperature gradients. The LIMS forward radiance model allowed a first approximation to the horizontal temperature gradient to be used to lead to improved temperature and constituent retrievals.

Local Thermodynamic Equilibrium (LTE)

The model assumes that CO_2 and O_3 are in LTE; that is, their energy levels are populated according to a Boltzmann distribution, so that the source function is given by the Planck function. On theoretical grounds (Houghton, 1969), and from ATMOS observations (Muggeridge, private communication), there appears to be no reason to question this for the 15 μm bands of CO_2 at altitudes below 80 km that materially affect LIMS radiances. However, O_3 may be photochemically formed in a vibrationally excited state, with several excess 9.6 μm quanta. This energy can be removed through quenching or radiation. Solomon et al. (1986b) have suggested that quenching is sufficiently slow that the source function is significantly greater than the LTE value above 0.5 mb. The various rates for these processes are uncertain, so the quantitative size of this effect is not precisely known. However, the calculations of Solomon et al. indicate that LIMS ozone is around 30 percent too large at 0.1 mb.

3.3.8.4 Inverse Method Assessment

The inversion procedure does not require a first-guessed profile; thus, the solutions are not biased to some a priori profile.

No noise covariance matrices are used in the inversion procedure. The solutions are derived exactly from the measured radiances, thus propagating any measurement error directly into the retrieved solution.

Retrieval Errors

A detailed error analysis on the LIMS ozone retrieval was performed through model simulations and retrievals (Remsberg et al., 1984). Table 2 in the referenced paper summarized the various error components and their magnitudes. The two dominating factors in the LIMS ozone retrieval uncertainty are the temperature uncertainty and the ozone line parameters uncertainty, which can (conservatively) produce retrieved ozone mixing ratio errors as high as 10–30 percent and 8–15 percent, respectively. The total retrieved ozone upper limit uncertainties were estimated to be 15 percent between 5 and 1 mb, and to increase to 40 percent at 100 mb and 0.1 mb.

Aerosols, PSC's, and high-altitude cloud interference should, in principle, affect LIMS data only at the height of the atmospheric perturbation. Most of these occurrences are removed by identifying their signatures in the moderately transparent ozone channel. The corrections in the frequency domain for sidelobe effects should remove the effects of high, cold, tropospheric clouds, but a small residual effect may be present. Volcanic aerosols were particularly low during the LIMS observing period.

3.3.8.5 Error Analysis

For LIMS, the state vector **x** is the ozone mixing ratio at levels spaced every 1.5 km on a grid for which the temperatures and pressures are known from the temperature–pressure retrieval. Correspondingly, the measurement vector **y** has as elements the emitted radiances on the same grid, smoothed and filtered as described above.

Averaging kernels for several altitudes are shown in Figure 3.25. The full width at half maximum is about 2.5 km.

Sensitivity to temperature errors at individual levels is shown in Figure 3.26. Figure 3.27 illustrates the total effect of a 1K temperature error at all levels, where the signs are opposite; i.e., a temperature that is low will result in a high ozone concentration. The temperature channels are used to derive a registration pressure; the effect of a 1 percent error in this quantity is also shown. Finally, the effect of a 1 percent calibration error is given. It should be emphasised that the error cases are somewhat simplified in that a calibration error probably would affect the temperature (and pressure) channels as well, and some cancellation of errors would result. The temperature and pressure errors here should be thought of as those that are not due to calibration errors and, because this relationship is not included, are illustrative rather than exact.

3.3.8.6 Trend Estimation Assessment

Trend estimation from the LIMS measurements will not be discussed here because of the short lifetime of LIMS operation (operated from October 1978 to May 1979), and because the retrieval algorithm is tailored to handle the particular engineering problems of LIMS, such as the

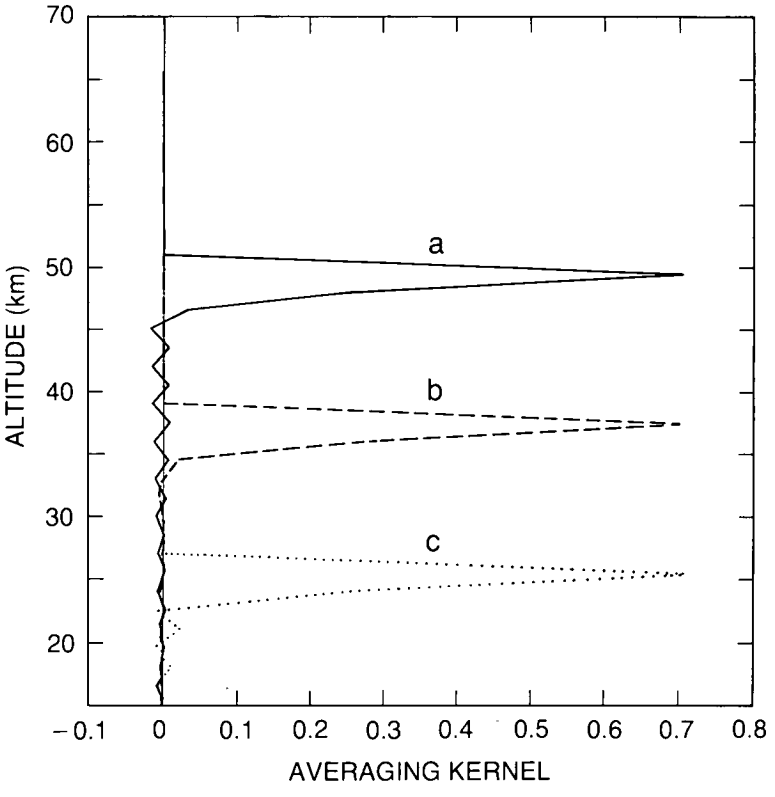

Figure 3.25. LIMS ozone averaging kernels at three selected altitudes.

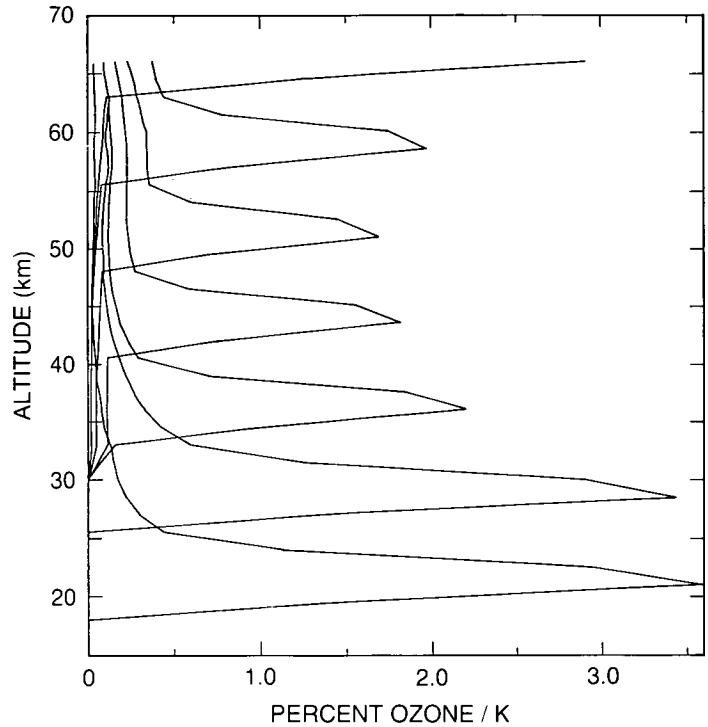

Figure 3.26. Sensitivity of LIMS-retrieved ozone to temperature errors at selected altitudes.

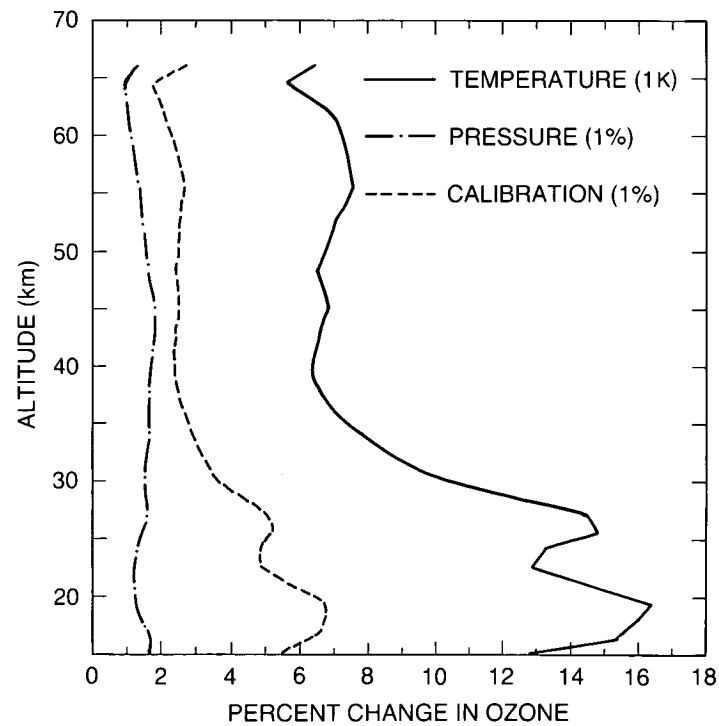

Figure 3.27. Sensitivity of LIMS-retrieved ozone to a 1K temperature change at all levels, a 1 percent radiance calibration error, and a 1 percent registration pressure error.

IFOV sidelobe problem, compounded with the spacecraft attitude uncertainty. As with most other measurement schemes, ozone trends sensed with a LIMS-type instrument would be susceptible to problems of instrument degradation; these can, in principle, be corrected for by in-flight calibration. However, for the LIMS type of measurement, temperature sensitivity is its biggest drawback since the source function and the species line parameters are dependent on the exact value of the atmospheric temperature. Thus, an undetected or wrongly retrieved temperature drift would lead to an erroneous ozone trend.

3.4 ALTERNATIVE STRATEGIES FOR OZONE PROFILE TREND DETECTION

The traditional method for looking for trends in remotely sensed ozone profiles has been the direct statistical analysis of the retrieved profiles on a layer-by-layer basis (e.g., see Reinsel et al., 1984). The retrieval methods generally have been designed to give the best results for individual profiles and may not produce optimal results for trend studies as a result of the relative weight given to a priori and measurement, for example.

In this section, we discuss possible alternative approaches for the detection of trends in ozone profiles. These include methods that involve the statistical analysis of the actual physical measurements, without direct recourse to a retrieval algorithm, and methods involving retrieval, but designed to retrieve trend profiles.

3.4.1 Analysis of Directly Measured Quantities

3.4.1.1 SBUV and Umkehr Measurements

We have examined the signature, in measurement space, of the postulated CFM ozone depletion centered near 40 km. Figure 3.28 shows the SBUV spectral signature, in terms of

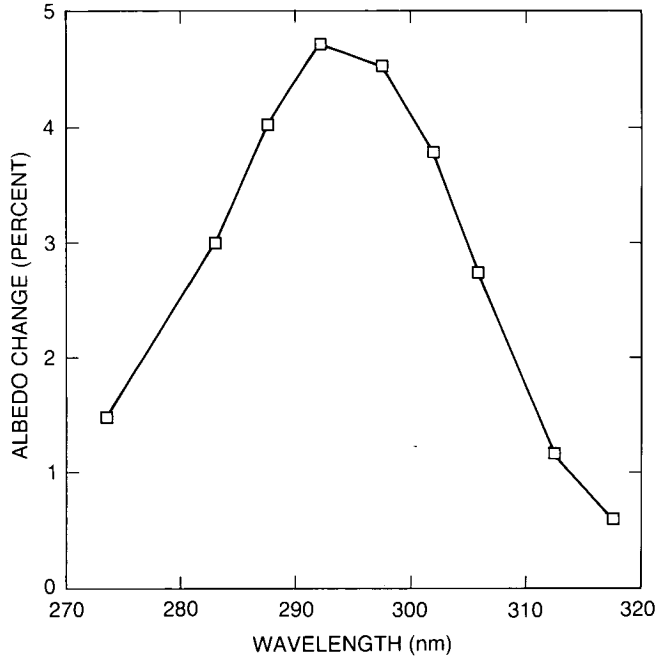

Figure 3.28. SBUV spectral signature for a Gaussian ozone depletion of 10 percent centered at 3 mb, with a width of 10 km at half maximum.

percentage albedo change, for a Gaussian shape percentage depletion centered at 3 mb, with a peak depletion of 10 percent and a width of 10 km at half maximum. This is a distinctive signature that is unlikely to be produced by either a wavelength-dependent drift in the reflectivity of the SBUV diffuser plate or by a small drift in the wavelength calibration (see Chapter 2). Since the overall shape of the SBUV spectral albedo curve depends on such factors as total ozone, season, latitude, solar zenith angle, and the multiple scattering and reflectivity "correction" to the observations, the analysis is not trivial. Moreover, the spectral signature of the profile depletion will also be somewhat dependent on these same factors. Finally, it would be necessary to distinguish between the spectral signature of this depletion and the stratospheric aerosols (Figure 3.2). Fortunately, this particular aerosol signature has a much narrower peak than the depletion signature. It is beyond the scope of this section to explore this potential method in full detail. However, it is evident that a good place to start would be with the initial preinversion, forcing residuals of the present SBUV algorithm, since the factors listed above are already largely removed from these residuals.

The curves joining the small squares in Figure 3.29 illustrate the Umkehr measurement-space signature of a similar Gaussian shape percentage depletion with, however, a maximum depletion of 25 percent and a half-width of about 14 km. Unfortunately, this signature is very similar to the stratospheric aerosol signature given by the curves joining the small triangles. Figure 3.29a is for a stratospheric aerosol optical depth of 0.0348, and for midlatitude ozone profiles with 200 matm-cm total ozone. The aerosol curve is taken from the data of Dave et al., 1979. Figures 3.29b and c show similar curves for midlatitude ozone profiles with total ozone of 300 and 400 matm-cm, respectively. For both the depletion and haze signature curves, the width of the signature increases and the amplitude decreases (only very slightly in the case of the depletion signatures) as the total ozone increases. It follows that any attempt to use this signature technique for the trend analysis of the Umkehr observations must deal appropriately with the problem of stratospheric aerosol contamination of the measurements, when such contamination exists.

With respect to calibration problems with the Dobson instrument, this alternative method appears to offer no particular advantage over the traditional method, because a wedge calibration error might very well have a signature similar to those in Figure 3.29.

In summary, this trend approach may offer some advantage when applied to SBUV data, but appears to offer little if any advantage with the Umkehr data. Only the broad, 40 km depletion has been examined here because other features of model-predicted ozone changes will be more difficult to find with either SBUV or Umkehr data.

3.4.1.2 SME–NIRS

An alternate method of obtaining ozone trends from the NIRS experiment on SME is to examine the airglow layer itself. This layer, which has a peak near 1 mb, is approximately a Chapman layer following the absorption of ultraviolet solar radiation. The radiance at the peak is primarily a function of the ozone density profile. With all other conditions being constant, long-term trends in its intensity would indicate ozone trends. The other parameters that influence the airglow peak intensity, and hence the peak radiance observed from the spacecraft, are solar zenith angle, tilt angle, and the ozone distribution. With a simple model, effects of solar zenith angle and tilt angle can be accounted for. Although a long-term change in the ozone distribution would be seen as a trend, it is, of course, an ozone trend—that is, there may be some ambiguity about the exact nature of the observed ozone trend. A remaining uncertainty is any

change in the sensitivity that has been measured by the inflight calibration. This method removes the largest source of uncertainty in SME–NIRS ozone, the altitude determination.

3.4.2 Trend Retrieval

Some of the observing systems use "optimal" retrieval methods. These are methods that attempt to minimise the error terms in the error analysis described in Section 3.2 on the basis of assumptions about the statistical behaviour of the instrument noise and the atmospheric profile.

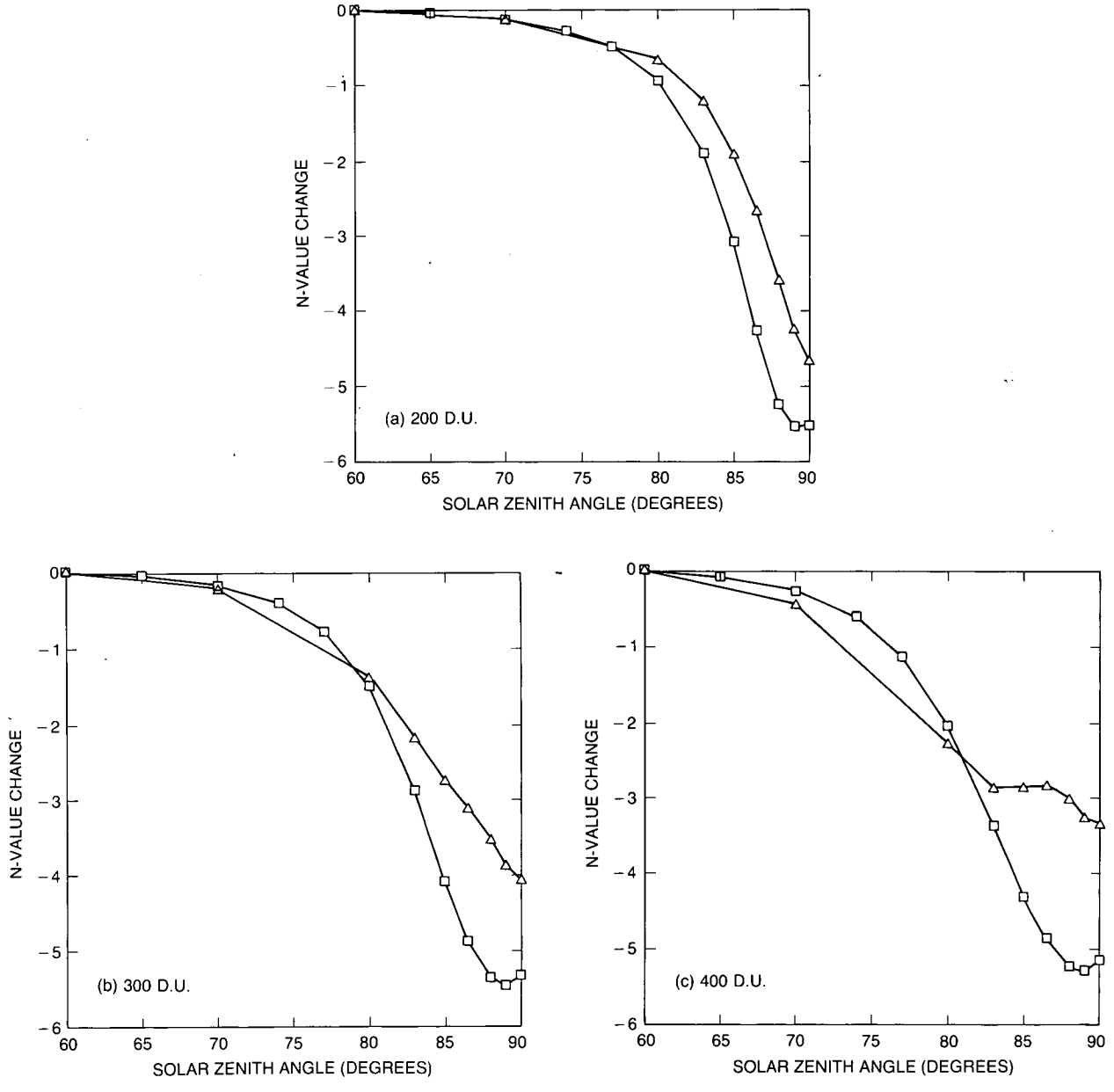

Figure 3.29. Umkehr measurement signature for a Gaussian-shaped depletion with a maximum of 25 percent and a half width of about 14 km centered at 3 mb (squares). Stratospheric aerosol signature (triangles). (a) Total ozone 200 DU. (b) Total ozone 300 DU. (c) Total ozone 400 DU.

These methods are usually designed to give optimal results for single profiles; consequently, they do not necessarily give optimal estimates when the retrieved profiles are used for long-term means or trend analysis. The user must be aware of the nature of optimal retrievals when carrying out statistical analyses.

Qualitatively, the optimal retrieval is a weighted mean of the true profile and an a priori profile, with the weighting depending on the measurement error

$$\hat{\mathbf{x}} = \mathbf{A}\mathbf{x} + (\mathbf{I} - \mathbf{A})\mathbf{x}^a \tag{46}$$

If the measurement error can be reduced, for example, by averaging, then the weighting should lean more toward the true profile and less toward the a priori.

The quoted error on a profile may include components from the error in $\mathbf{x}^a$ as well as those due to experimental error. Only the latter varies from one profile to the next.

It should be possible, in principle, to retrieve trends over a greater height range and with better resolution than that obtainable from individual retrievals because random errors in the data are reduced by averaging. This is straightforward in the case of linear forward models because the measurements can be averaged directly to remove noise. In the nonlinear case, it is more difficult; further research is needed to set up a sound basis for trend retrieval.

We note that, as random errors are reduced, systematic errors with trends become more important and need more careful treatment.

3.5 SUMMARY AND CONCLUSIONS

We have found no serious deficiencies in the algorithms used in generating the major available ozone data sets. As the measurements are all indirect in some way, and the retrieved profiles have different characteristics, data from different instruments are not directly comparable. Thus, the primary aim of this chapter has been to characterise the algorithms to show quantitatively:

- How the retrieved vertical profile is related to the actual profile. This characterises the vertical resolution and altitude range of the data.
- How trends in the real ozone are reflected in trends in the retrieved-ozone profile.
- How trends in other quantities, both instrumental and atmospheric, might appear as trends in the ozone profile.

3.5.1. Error Analysis Concepts

Error analyses for the ozone data sets that we have considered have, in general, been published in the open literature, but not in a uniform and comparable way. We have, therefore, defined a uniform error analysis approach and applied it to all of the data sources. The formal error analysis shows that the retrieved vertical profile $\hat{x}(z)$ can be expressed as an explicit function of the true profile $x(z)$, plus error terms due to instrument noise and systematic errors. This

function can be thought of as a smoothing of the true profile with a smoothing function we call the *averaging kernel* $A(z, z')$:

$$\hat{x}(z) = \bar{x}(z) + \int A(z, z')(x(z') - \bar{x}(z'))dz' + \text{error terms} \quad (47)$$

The range of height z over which the averaging kernel has a well-defined peak determines the height range of validity of the retrieved profile, while the width of the peak defines the vertical resolution of the profile. The error terms due to various sources can be examined independently. Those leading to constant offsets, or purely random errors, are of minor importance when studying trends, as random errors will average out in the long run and constant offsets make no difference to trend estimates. The most important sources of error are those that have trends themselves, which might appear as false trends in ozone.

The range of validity and vertical resolution of the ozone data sets that have been available to the Ozone Trends Panel are given in Table 3.6. Also listed are the primary sources of systematic error that may introduce incorrect trends into the retrieved data.

Table 3.6 Summary of Retrieval Characteristics

Instrument	Altitude Range*		Resolution	Sources of Trend Error
	mb	km	km	
SBUV	16-1	(28-50)	8-10	Diffuser plate reflectivity, aerosol.
Umkehr	64-2	(19-43)	11-14	Aerosol, sampling.
SAGE–I	(250-1)	10-50	1	Aerosol below 25 km, sampling.
SAGE–II	(250-1)	10-50	1	Aerosol below 25 km, sampling.
	(1-0.1)	50-65	5	
SAGE–II/–I	(250-1)	10-50	1	Altitude reference, filter placement.
SME–UVS†	(1-0.05)	48-68	4	UVS and Solar Flux instrument calibration, pressure at 68 km, mesospheric aerosol?
SME–NIRS	0.3-0.003	(55-85)	4-10‡	Altitude reference, calibration, atmospheric temperature.
LIMS	100-0.1	(15-64)	2.5	(short record)

*Brackets indicate approximate equivalent
†Experimenters assessment.
‡Varying with time

3.5.2 Individual Data Sources

3.5.2.1 Dobson Total Ozone

The only algorithmic source of trend error is the omission of the effects of SO_2, which itself has a trend. Stratospheric aerosol, which has variability on a long time scale, is also omitted.

3.5.2.2 TOMS and SBUV Total Ozone

The primary source of error here is the spectral variation of the drift in diffuser plate reflectivity. The range of reasonable models of this drift presented in the calibration chapter leads to a possible overestimate of around 3–4 percent in the ozone depletion over the 8-year data period. A minor source of trend error is an underassessment of tropospheric ozone by a factor of about two.

3.5.2.3 SBUV

Although the archival data cover Umkehr layers 1 to 12 (altitude range approximately 0–64 km), we find that only layers 6 to 9 or 10 (28–50 km) are suitable for trend analysis. The sensitivity of the retrieval to diffuser plate reflectivity errors has a similar vertical profile to the global trend seen in SBUV Version 5 data. Uncertainty in this trend due to errors in the diffuser plate reflectivity within experimental error is comparable with the trend itself.

3.5.2.4 Umkehr

The archival data cover an altitude range of layers 1 to 9 (0–48 km). We find that only layers 4 to 8 (19–43 km) are suitable for trend analysis. There are many sources of systematic error that affect an individual instrument in a way that varies with time, such as recalibration and operator competence. The network is not large enough to rely on these effects averaging out in the long run. We note also that aerosol effects and temperature dependence are not allowed for in the retrieval.

3.5.2.5 SAGE

SAGE has an excellent vertical resolution, but a poor sampling frequency. This means that care must be taken in deriving statistically valid trends. We have found no problems that might lead to trend errors when using data from one instrument, other than its sensitivity to aerosols below about 25 km. When comparing SAGE–I with SAGE–II, it must be remembered that the systematic errors in the two data sets are likely to be different. Specifically, the different treatment of the reference altitude can lead to a systematic difference increasing with height; errors in filter placement can lead to scale errors, differing between the two instruments. It should also be noted that, as SAGE measures on a height scale, while SBUV measures on a pressure scale, temperature trends must be correctly modeled when comparing trends from these two instruments.

3.5.2.6 SME

The vertical resolution of the retrieval from both the UVS and the NIRS degraded with time as the attitude of the spacecraft changed. The primary source of trend errors for both instruments is the altitude reference. The NIRS retrieval relies on a complete understanding of the relevant photochemistry, including its temperature dependence. We have found no errors, but it is quite possible that some chemistry has been omitted or misunderstood.

3.5.2.7 LIMS

We have found no significant sensitivities that might influence trend assessment. However, the measurement period is rather short, so that LIMS has little to say about trends. Its main value here is to validate other data sources.

3.5.3 Discussion

In view of the above characterisation of the various sources of data, it is clear that comparisons should be made only over the range of validity of the individual data sets, at comparable vertical resolutions, degrading the higher resolution data as necessary. It would be helpful for

future exercises of this kind if data suppliers could present a standard set of observing system characteristics, perhaps based on those developed for this report.

Retrieval methods appropriate to trend estimation are not necessarily the same as methods appropriate to estimation of single profiles because it may be possible to largely eliminate random error in the long-term averages required for trends. However, the retrieval methods used for the data now available are designed for single profiles. Further research is needed to design trend profile retrieval methods.

An alternative approach to trend detection is to look for changes in the quantity actually measured, without retrieving a profile. Modeled changes in the ozone distribution can be used with the forward model for a particular instrument to determine whether the resulting perturbation in the quantity measured is detectable.